MODEL BASED STRUCTURAL MONITORING OF PLATES USING KALMAN FILTER

by

Dyan Melvin

A Thesis Submitted to the Faculty of the

DEPARTMENT OF CIVIL ENGINEERING AND ENGINEERING MECHANICS

In Partial Fulfillment of the Requirements

For the Degree of

MASTER OF SCIENCE

In the Graduate College

THE UNIVERSITY OF ARIZONA

2016

STATEMENT BY AUTHOR

The thesis titled *Model Based Structural Monitoring of Plates using Kalman Filter* prepared by *Dyan Melvin* has been submitted in partial fulfillment of requirements for a master's degree at the University of Arizona and is deposited in the University Library to be made available to borrowers under rules of the Library.

Brief quotations from this thesis are allowable without special permission, provided that an accurate acknowledgement of the source is made. Requests for permission for extended quotation from or reproduction of this manuscript in whole or in part may be granted by the head of the major department or the Dean of the Graduate College when in his or her judgment the proposed use of the material is in the interests of scholarship. In all other instances, however, permission must be obtained from the author.

SIGNED: *Dyan Melvin*

APPROVAL BY THESIS DIRECTOR

This thesis has been approved on the date shown below:

Hongki Jo
Assistant Professor of Civil Engineering

4/27/2016
Date

Table of Contents

List of Figures

List of Tables

ABSTRACT

Structural health monitoring (SHM) is a quickly advancing field of study in civil engineering and recent advances in the field are in stark contrast to where the field started. For example modern technology of wireless sensing systems allowed for easier monitoring of structures, but the challenge of limiting the number of instrumented locations has not been overcome with traditional methods. The potential of alternative methods has only been realized in recent years with the increase of model based approaches. In particular, the use of limited measurements to estimate structural response at all locations is appealing. To accomplish this goal, this work approaches SHM by using a numerical model combined with a linear recursive state estimation algorithm, known as the Kalman Filter, to update the model-based prediction with a limited number of real time measurements taken on the structure. A thorough overview of the contents is given here. The first section introduces the topic of SHM and the goal of SHM. Then the challenges and limitation that face SHM are discussed along with the recent advances that can be used to overcome them. In Section 2, the proposed framework, a Kalman filter approach, is established. First, a finite element model is formulated for plate structures using the Mindlin-Reissner plate theory and then this finite element code is verified by a comparison with a commercial FEA software. Then the state space model of the system is defined for use with the Augmented Kalman Filter (AKF); the AKF approach overcomes the intrinsic challenge of unknown excitations for civil structures. The AKF is then formulated and discussed. For Section 3, using the AKF in numerical simulations are conducted for 5 different cases. The first three cases study the advantages of multi-metric measurements, i.e. strain and acceleration measurements combined, versus single metric measurement, i.e. strain measurement only or acceleration measurement only. Following that, the next two cases explore the question of whether multi-metric measurements will always provide

the best results. Based on the conclusions from the previous section, Section 4 investigates the application of a genetic algorithm, a search algorithm based of Darwinian principles, to find the optimal sensor placement to use as the input to the AKF. Here the developed search algorithm is used in two cases, the first is to find the optimal placement for the strain measurement only case. Next, the improvements in accuracy that are gained by placing taking more measurements is investigated to determine if the gain in accuracy per added measurement decreases for large numbers of measurements. Section 5 contains the final conclusions about the use of the AKF for SHM of plate structures then the potential opportunities of future work regarding plate structures are discussed.

1 Introduction

Structural health monitoring (SHM) is a diverse area with work persisting in many fields such as mechanical engineering, aerospace engineering, and civil engineering. The principal purpose of SHM is to accurately estimate structural health as a tool that can better inform decisions regarding structures. This primary objective is important because if it can be meet then there will be a significant impact on the way structures are designed, understood, and maintained. The advantages of having a well-defined SHM method are clear especially in the field of civil engineering where this work is focused.

The advantages that can be achieved include a reduction in the number of costly repairs as problems are able to be caught at an earlier stage and this can further benefit structures by prolonging their life. However, the main benefit is the increased reliability of the structures since the structures can be proactively monitored to determine if dangerous conditions, e.g. loading or fatigue, has or is occurring, and if necessary call for the closure or inspection of structures. In the overall picture this type of smart monitoring can lead to fewer catastrophic accidents that cause property damage and loss of life. Preferably, a well-developed SHM method can be used to provide real-time monitoring of structures to help prevent structural failures and undoubtedly, this type of understanding is beneficial. However, the challenge of SHM lies in its definition which can be very ambiguous.

This ambiguity is related to the very general and all-encompassing idea that SHM can take. People will often broadly define SHM as a comprehensive practice that includes all the technology,

hardware and software, for sensing and additionally, the algorithms, metrics, or methodologies that are used for analysis. This analysis should include all states of the structure as it goes through its life cycle and this life cycle is quite complex including the construction, operational and future performance of the structure. Many of these topics, e.g. sensing technologies, have their own subfields of research but for a general overview of SHM one can use the following references: Doebling et al. (1996), Farrar (2001), Sohn et al. (2003), and Brownjohn (2007).

As for why SHM has been receiving an increasing amount of attention is not an easy question to answer but the fact is that many countries are becoming developed, i.e. the built environment of these countries continues to grow. This development means that there is an ever increasing number of newly built and aging infrastructure around the world and they are demanding for SHM research to catch up. An example of this demand is shown in the U.S. by a response from the Federal Highway Administration (FHWA) which created a program with the goal of creating a next-generation, integrated framework because as the FHWA stated "fiscally responsible, safe, life-cycle management of the Nation's bridges depends on reliably predicting their health over time." (FHWA, 2012) This demand will continue to grow and so does the potential body of research for SHM.

1.1 Conventional structural health monitoring

The conventional SHM approach is to monitor the structure through the use of regularly scheduled inspections. These inspections usually consist of a visual rating system which includes using a scale of 1 to 10, with 1 being a poor rating and 10 being an excellent rating, to indicate the status

of different structural elements, e.g. paving. This type of conventional SHM has many drawbacks. First of all, the inspection is highly subjective based on the inspector's experience and the inspector is only able to inspect what they can see and/or access which adds to the problem and makes the process even more subjective and inconsistent. Also, this process has a high cost and maintaining an inspection schedule can be difficult due to time constraints and the required manpower.

As technology has progressed, the development of sensors, e.g. strain gauges and accelerometers, presented the opportunity for SHM to be improved on. The early use of sensors in SHM saw the placement of sensors at as many locations as possible. Then the acquired data directly gave an indication of the structure's health for the location where they were placed. This approach is limited by the sensor's placement since for any measurement of interest, e.g. displacement or acceleration, it was required to have a sensor placed directly at that specific location and monitored though time to get the necessary data. Therefore, it is obvious that this approach relies heavily on the physical measurements and a large number of sensors are required if one hopes to get a good sense of the overall structural health.

Furthermore, several limitations of this practice have been discovered when the implementation of a physical sensing based SHM was tried for several field structures. The field deployment of sensor networks particularly highlighted the challenge of instrumenting large civil structures and accurately obtaining the information from sensors. A key part of the challenge is the installation and maintenance of the wired instrumentation which has a high cost and can be difficult to place at all necessary locations on the structures. (Lynch and Loh, 2006) Another challenge is the

information obtained can be noisy and accessibility may be an issue that forces information to be gathered from a limited number of locations on the structure.

Recently, the advancement of wireless sensors and networks is helping to alleviate the challenges that faced traditional wired sensors. These new wireless sensors and networks are now widely used since they allow for easier placement of sensors without the need to run wires across the structure to connect sensors to the data repository. Other advances in the wireless sensing field include creating high performance sensors to capture the necessary information and at reduced noise levels. Future work is being done to research wireless systems that can be robust and self-powered. (Jang et al., 2010, Lynch and Loh, 2006, Spencer et al., 2004, Spencer et al., 2015)

Unfortunately, the use of wireless systems on their own are not able to address the challenge presented by the sheer size of civil structures; in particular, the improbable goal of placing a sufficient number of sensors on the structure to be able to measure all the states of structural response that are needed to use conventional SHM. This challenging problem persuaded researchers to use model based approaches.

1.2 Model based approach

To solve the problem of SHM for large structures, researchers have turned to a model based approach. One of the most popular model based approaches can be termed model identification. Model identification has been experimented with since the 1970s and used for a variety of applications in the civil field. This method works to detect a change in the characteristics of the

structure and to use that change to find the location of damage. The methodology is to detect damage as early as possible but an unfortunate limitation of the method is that damage must occur for this method to detect it. Usually the method looks at shifts in the frequency response of the structure as the structural characteristic to determine whether damage has occurred. As mentioned this approach has been popular with researchers for some time and it has been extensively developed. However, model identification has not been able to consistently provide good results. Some of the well-known challenges that face this method are in regards to whether the sensitivity of the structural characteristics is good enough to detect small or local damage, also the dependence of the method on a measurable input excitation, and reliance on a detailed model. For a good overview of these methods can be found in Doebling, 1996 which is provided as a reference. (Doebling et al, 1996)

Some other model based approaches work to compute fatigue or reliability metrics through the use numerical modeling and damage accumulation rules. (Fatemi and Yang, 1998, Kuhn et al., 2008, Zhou, 2008) This allows the potential locations that have the highest risk of fatigue to be found and then sensors would be placed at them to measure response. However, these methods can be unreliable for civil application since the loading conditions may be variable, inconsistent, and have a non-zero mean to them, this along with unanticipated structural behavior may cause damage in unmeasured locations.

To overcome the challenges of using the model based approach, several alternative methods for analysis have been pioneered that can make use of a limited number of measurements but

effectively estimate all the states of the structural response and these estimates include unmeasured states.

1.3 Kalman filter approach

One of these alternative methods that has good potential uses a hybrid approach which takes a numerical model (i.e. finite element model) and combines it with a limited number of real measurements taken from sensors on the structure. This method is then able to create a fusion between the numerical model and input of real measurements by using a linear recursive state estimation algorithm, known as the Kalman filter (KF).

The main advantage of this method, that can be termed state estimation, is that it works to obtain all the states, i.e. displacement, acceleration, etc., of the structural response based on the input provided by a limited number of real measurements. Since this method is able to give all the states it is then possible to find secondary unknowns like strain or stress and a time history can be computed for the structure. Once a time history of strain or stress is available, there are existing practices can be used to evaluate the overall health of the structure, i.e. find fatigue locations or identify stress concentrations, and develop metrics of reliability or fatigue. This state estimation method has the potential advantage, given proper development , to predict dangerous levels of fatigue before damage occurs and does not rely on having damage occur in order to detect it.

The use of the KF can be particularly advantageous for civil applications for several reasons. First, the filter is able to operate using a limited number of measurement inputs. Secondly, it is a robust

filter that can be constructed to include terms that account for process/model error and measurement noise. This makes it resilient to practical application in the field where the model error and measurement noise are almost certain to occur. Third, it is able to combine the model with different types of measurements, i.e. strain and acceleration or displacement and acceleration measurements. These combinations take advantage of the different types of measurements and is termed multi-metric measurements.

For the applications here, civil structures, it is important to once again consider the difficulties in instrumenting them. This difficult has influenced the choice of measurement type to tend towards sensors that can be easily placed. In general, the use of low-cost, easy-to-use, and reference-free sensors, i.e. strain gauges and accelerometers, are the most appealing. Of course, other measurements are possible to be used with the KF but measuring the displacement, for example, would require expensive vison based equipment or a static reference point. Neither of these are feasible for long term monitoring. Additionally, the use of strain and acceleration measurements as the multi-metric input for the KF in previous research has shown that local and low frequency information from strain along with the global and high frequency information from acceleration provides complementary information that is beneficial when combined.

Previously published research (Jo and Spencer, 2014, Lourens et al., 2012, Papadimitriou et al., 2011, Palanisamy, 2015) has been able to validate the use of the Kalman filter while using multi-metric measurements as the input for estimating some aspects of structural response for limited types of structures such as beams and trusses. However, there are many areas that remain to be studied. One area of interest that remains untouched is the use of KF for plate structures. In the

next section the importance of this structural element will be discussed and how the KF approach can be applied.

1.3.1 Plate structures

Plate structures are a common structural element that is used to connect members at joint locations. In design, plate structures used at joint locations are commonly called gusset plates. Gusset plates can be fastened to a permanent member either by bolts, rivets, welding, or a combination of the three. Plates can be made into a variety of shapes and sizes from a range of materials. These plates not only serve as a method of joining steel members together but they can also be used to strengthen the joint. Plates provide an easy way to retrofit structures that can no longer safely support the applied loads. A plate can be the only connection method or it can be used in conjunction with bolts or welds made directly between members. Plates are usually square or rectangular, but they can be made into a customized shape to fit the joint. The shape of each plate is designed so that welding or bolts can be applied to different edges of the plate. It is clear that plates are a fundamental part of structures and provide continuity to the structure. The calculations used to design plates are based upon the forces and loads applied to the gusset plate through the connected steel components. Well known research into the nature of plates was studied by R.E. Whitmore in 1952 and led to development of the Whitmore section which is used in modern design. (Whitmore, 1952) However, plates are still not understood as clearly as other structural members which can be analyzed and designed to a high degree of accuracy.

There are clear examples where a misunderstanding of the plate element lead to the catastrophic failure of the entire structure. The I-35W Bridge in Minneapolis is one of the better known examples where failure of the entire structure began from local plate failure. Sixteen plates were under-designed when they should have been larger sizes to be in accordance with the American Association of State Highway and Transportation Officials (AASHTO) "Standard Specifications for Highway Bridges," 1961. The post-collapse report from the National Transportation Safety Board concluded that the majority cause of the bridge failure was due to this flaw. (Hill et al., 2008) Following the incident, the FHWA advised states to inspect the 700 U.S. bridges of similar construction after a possible design flaw in the bridge was discovered related to gusset plates. The FHWA expressed concern about many other bridges in the United States which shared the same design and questioned why such a flaw would not have been discovered in over 40 years of inspections. (Wright, 2007)

The danger of failure due to issues arising at the plate elements is not limited to bridges. The current Green Bank Telescope at Green Bank, West Virginia, completed in 2000, was built following the collapse of the previous Green Bank telescope, a 90.44 m paraboloid constructed in 1962. The previous telescope collapsed on 15 November, 1988 due serious fatigue damage of a large gusset plate in the box girder structure, which was a key component for the structural integrity of the telescope. (Ayzazyan, 1989) These examples demonstrate the importance of the gusset plate for maintaining continuity in the structural system. Despite the importance of plate structures for a structural system, they can be poorly understood thus making them susceptible to failure.

The purpose of the research is to overcome the challenges facing SHM by taking advantages of new technology and methodologies. The use of a Kalman filter approach is one of the alternatives that is showing potential application to SHM. In particular this research identified plate structures as a structural element of significant importance but where there is a lack of understanding that has led to several significant structural failures. Furthermore, the application of a SHM methodology specifically for plate structures in the civil field is absent from the literature. The proposed approach can help further the idea of SHM and improves upon the existing knowledge of plate structures. Therefore, it is proposed that the augmented Kalman filter (AKF), a linear recursive state estimator, which provides statistically optimized state estimates for all locations including unmeasured locations based on a limited number of input measurements can be applied to plate structures. The filter is then able to estimate the three components of the in-plane strain, i.e. ε_x, ε_y, and γ_{xy}. The strain values are chosen to be estimated since strain time histories can be used for fatigue assessment.

A brief overview of the remaining sections is given here to explain the trajectory of the research. In Section 2, the framework of the proposed Kalman filter approach is established. First, a finite element model is formulated for plate structures using the Mindlin-Reissner plate theory and then this finite element code is verified by a comparison with a commercial finite element analysis software. The static and dynamic properties of the model are demonstrated. A detailed explanation is given for the strain-displacement relationship for this model since this relationship will be used as part of the AKF. The system is then required to be modeled in state space for use with the AKF. Finally, the details of the filter are formulated and discussed.

For Section 3, the AKF is used in numerical simulations to conduct 5 different scenarios. The first three cases study the advantages of multi-metric measurements, i.e. strain and acceleration measurements combined, versus single metric measurement, i.e. strain measurement only or acceleration measurement only. Following that, the next two cases explore the question of whether multi-metric measurements will always provide the best results and discuss the limitations that are found.

Based on the conclusions from the previous section, Section 4 investigates the application of the genetic algorithm, a search algorithm based on Darwinian principles, to find optimal sensor placements that will be used as the input to the AKF. The developed search algorithm is used in two cases, the first is to find the optimal placement for the strain measurement only case. In the next case, the increase in strain estimation accuracy gained by taking more measurements as input to the AKF is investigated to determine if there is a finite number of measurements that should be used.

The last section, Section 5, contains a summary and final conclusions about the use of the AKF for strain estimation of plate structures. Finally, the potential opportunities for future work are discussed.

2 Model-based monitoring for plate structures

For the AKF formulation, it requires the system to be described via a state space model. Therefore, the initial step is to construct the mass ($\boldsymbol{M}$), damping ($\bar{\mathbf{C}}$), and stiffness ($\boldsymbol{K}$) matrices of the plate structure using a finite element formulation. These matrices are necessary to represent the system which in the simulated cases is a cantilever plate. After the system was defined in state space, two known input excitations can be applied to obtain a complete time history and the simulated sensor measurement data. Further manipulation of the state space representation is needed to get the augmented state space before the AKF can be formulated. This filter, as previously described, is a linear recursive state estimator which follows a predictor-corrector form to get statistically optimized strain estimates for all locations. The figure below shows the basic augmented Kalman filtering process that is used.

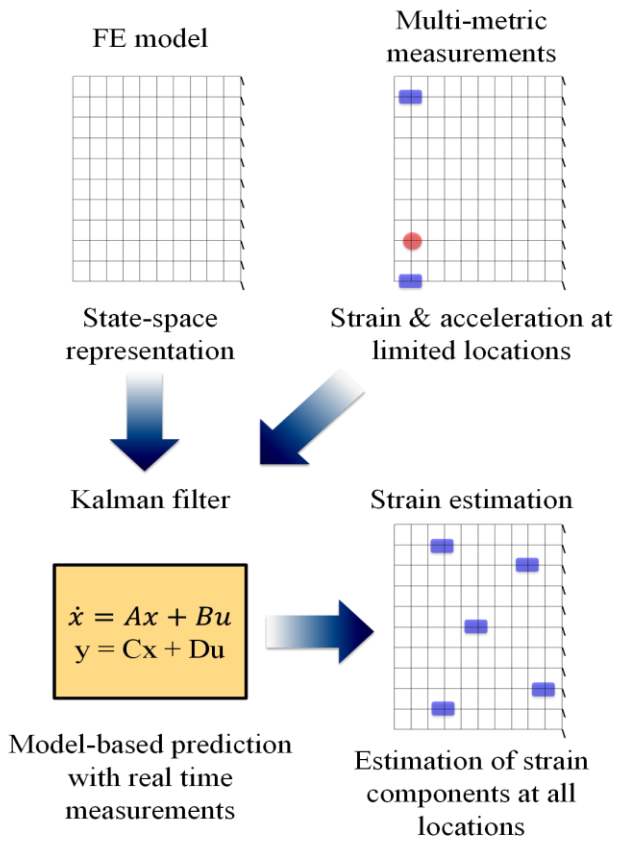

Figure 1: Augmented Kalman filter process

From the above figure, it is seen that the AKF requires two inputs. The first is the structural system which is to be modeled in state-space using a finite element model. The second input is the real structural measurements, i.e. strain and acceleration. The filter is then able to combine these two inputs to produce model based predictions that are updated with real time measurements. From the predictions, strain can be calculated for all strain components at all locations throughout the plate.

In the following sections, each individual step needed for the filtering process is described in more detail; starting with the finite element theory that was used to model the plate. Then followed by the state space model and, finally, the augmented Kalman filter.

2.1 Finite element model for plate structures

The Mindlin-Reissner plate theory, or commonly called Mindlin plate theory, is used to create the finite element model. This theory was developed to study the bending and shearing behavior of thick plates. (Bathe, 1982) It is similar to the Kirchoff-Love plate theory with the key difference being that Mindlin plate theory does not assume that plane sections remain plane but it does assume that the sections remain straight. This difference in the theories means that the Mindlin plate formulation is useful for studying thick plates since it incorporates first-order shear deformations and in-plane shear strains. It is beneficial to use the Mindlin plate theory for the analysis because it is not unusual to have a thick plate used in a civil engineering application; though plate sizes can vary significantly based on the specific application, i.e. design forces. Highway bridges may have plates with thickness to width ratios close to 0.025, while in contrast, a building application may have a ratio closer to 0.07.

The Mindlin plate theory was implemented using MATLAB as the primary programing language to construction the finite element model. The code was written following the finite element notation used by A.J.M. Ferreira in "MATLAB codes for finite element analysis: Solids and structures". (Ferreira, 2008) The elements were taken as quadrilaterals with four nodes; each having three degrees of freedom: w_z, θ_x, and θ_y. These three dofs, one displacement and two rotations, are the primary unknowns. The stiffness matrix was constructed starting from the linear elastic stress-strain relations for a homogeneous, isotropic material which can be used to define the strain energy considering the flexural and shear contributions. Once the strain energy was defined the stiffness matrix was obtained from reduced integration considering 2x2 Gauss points

for the bending contribution and 1 point for the shear contribution. Reduced integration is recommended as one of the simplest methods to avoid the shear locking problem in plates. (Bathe, 1982) The mass matrix was constructed using the consistent mass matrix method, where the same shape functions that were used in the stiffness derivations are again used for constructing the mass matrix. The finite element formulation for plates using Mindlin plate theory is thoroughly covered in the literature, see Ferreira for details. (Ferreira, 2008)

Since strain estimation is the key to the research and adoption of the strain-displacement relationship into the AKF was needed it is useful to explain the details of relationship from the finite element model. As mentioned the Mindlin plate theory can be used to calculate the strain values, a secondary unknown, via the strain-displacement relationship which will be shown here. The strain-displacement relationship is derived starting from the local node numbering and local coordinates for the quadrilateral element as shown here.

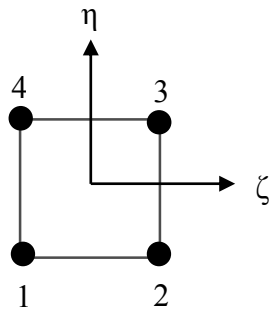

Figure 2: Local node numbering and local coordinates for quadrilateral element

The vector $\boldsymbol{u}(t)$ shown below is the vector of the displacement values for the local nodes of the quadrilateral element.

$$\boldsymbol{u}(t) = \begin{Bmatrix} w_1(t) \\ \theta_{x1}(t) \\ \theta_{y1}(t) \\ \vdots \\ w_4(t) \\ \theta_{x4}(t) \\ \theta_{y4}(t) \end{Bmatrix} \tag{1}$$

Now the equation below shows $\boldsymbol{B_f}$ which is the strain-displacement matrix for the flexural contribution.

$$\boldsymbol{B_f} = \begin{bmatrix} 0 & \frac{\partial \mathrm{N}_1}{\partial \mathrm{x}} & 0 & \cdots & 0 & \frac{\partial \mathrm{N}_4}{\partial \mathrm{x}} & 0 \\ 0 & 0 & \frac{\partial \mathrm{N}_1}{\partial \mathrm{y}} & \cdots & 0 & 0 & \frac{\partial \mathrm{N}_4}{\partial \mathrm{y}} \\ 0 & \frac{\partial \mathrm{N}_1}{\partial \mathrm{y}} & \frac{\partial \mathrm{N}_1}{\partial \mathrm{x}} & \cdots & 0 & \frac{\partial \mathrm{N}_4}{\partial \mathrm{y}} & \frac{\partial \mathrm{N}_4}{\partial \mathrm{x}} \end{bmatrix} \tag{2}$$

Where $\boldsymbol{N_i}$ from the strain-displacement matrix is the Lagrange shape functions given below for a quadrilateral in natural coordinates, ($\boldsymbol{\zeta}$, $\boldsymbol{\eta}$) shown in Figure 2, for $\boldsymbol{i}$ = 1,2,3,4.

$$\boldsymbol{N}_i = \frac{1}{4}(1 + \boldsymbol{\zeta\zeta_i})(1 + \boldsymbol{\eta\eta_i}) \tag{3}$$

Then the final equation below shows the strain-displacement relationship for the in-plane strain components, ε_x, ε_y and γ_{xy}.

$$\boldsymbol{\varepsilon}(t) = \begin{Bmatrix} \varepsilon_x \\ \varepsilon_y \\ \gamma_{xy} \end{Bmatrix} = \boldsymbol{B_f u}(t) \tag{4}$$

The relationship shown in Eqn. 4 between the displacement field and the in-plane strain components will be used in the AKF observability matrices to modify the strain selection matrix and used to calculate the in-plane strain components from the estimated displacement states given by the AKF.

2.1.1 Verification of finite element model

The finite element model developed in MATLAB was verified against SAP2000, a commercially available finite element analysis software. The figure below shows the cantilever plate setup and the location of the applied static load that was used in the comparison.

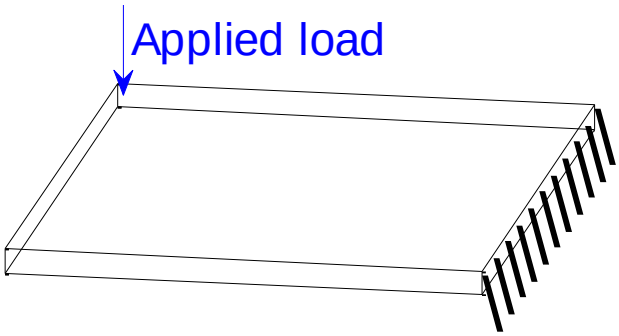

Figure 3: Cantilever plate with applied static load

This setup was chosen because it closely resembles the conditions that may exist for a gusset plate and has the same boundary conditions that will be used in the other simulations. The following dimensions were used: 40.64 cm (16 inches) by 30.48 cm (12 inches) by 0.3175 cm (1/8 inches) thick. The material properties were chosen to be identical to those of A36 steel. Young's modulus equal to $200x10^9$ Pa and density of 7800 kg/m^3. For the boundary condition one of the longer sides, i.e. 40.64 cm, was fixed and the other three sides are free. A force of 2224.1 N (500 lb-f) was applied at the free corner as shown by the arrow in Figure 3. Then the finite element analysis in both programs was conducted using a 20 by 20 element mesh of quadrilateral elements.

The results of the analysis then gave two parameters that were compared. The first parameter is the maximum displacement value, which occurs at the location of the applied load as expected, and the second parameter was the natural frequency of the plate. These two parameters were

chosen because they represent the static properties and the dynamic properties of the plate. The table below contains the results of the two analyses.

Table 1: Comparison of developed Matlab code vs SAP2000

	MATLAB		**SAP2000**	
MODE	Frequency (Hertz)	Displacement (Inches)	Frequency (Hertz)	Displacement (Inches)
1	28.926	6.1788	28.898	6.1612
2	57.375		57.338	

As shown in the table the results of the two analyses match quite well. These results validate that the developed MATLAB code is working correctly and can be used in the state space representation.

2.2 State space model

To get the state space model, one can start from the equation of motion for a linear dynamic system can be given as:

$$\boldsymbol{M}\ddot{\boldsymbol{u}}(t) + \bar{\mathbf{C}}\dot{\boldsymbol{u}}(t) + \boldsymbol{K}\boldsymbol{u}(t) = \boldsymbol{S}_p\boldsymbol{p}(t) \tag{5}$$

Where $\boldsymbol{M}$, $\bar{\mathbf{C}}$, and $\boldsymbol{K}$ are the mass, damping, and stiffness matrices, respectively. $\boldsymbol{u}(t)$ is the displacement as a function of time; $\dot{\boldsymbol{u}}(t)$ and $\ddot{\boldsymbol{u}}(t)$ are the time derivatives which are velocity and acceleration, respectively. $\boldsymbol{p}(t)$ is the input excitation vector and $\boldsymbol{S}_p$ is the force selection matrix. $\boldsymbol{S}_p$ is formed so that if "**n**" is the number of degrees of freedom for the system than $\boldsymbol{S}_p$ has the size

"**n x n_p**" where **n_p** is the number of degrees of freedom where the input excitation is applied and in general "**n_p < n**". Now the state space model can be formed.

Letting $\boldsymbol{x}(t)$ equal the state vector:

$$\boldsymbol{x}(t) = \begin{Bmatrix} \boldsymbol{u}(t) \\ \dot{\boldsymbol{u}}(t) \end{Bmatrix} \tag{6}$$

The equation of motion can then be expressed as a state space model having the form

$$\boldsymbol{x}(t) = \boldsymbol{A}\boldsymbol{x}(t) + \boldsymbol{B}\boldsymbol{p}(t) \tag{7}$$

$$\boldsymbol{y}(t) = \boldsymbol{C}\boldsymbol{x}(t) + \boldsymbol{D}\boldsymbol{p}(t) \tag{8}$$

The matrices $\boldsymbol{A}$ and $\boldsymbol{B}$ can be defined as

$$\boldsymbol{A} = \begin{bmatrix} \boldsymbol{0} & \boldsymbol{I} \\ -\boldsymbol{M}^{-1}\boldsymbol{K} & -\boldsymbol{M}^{-1}\bar{\mathbf{C}} \end{bmatrix} \quad \boldsymbol{B} = \begin{bmatrix} \boldsymbol{0} \\ \boldsymbol{M}^{-1}\boldsymbol{S}_p \end{bmatrix} \tag{9}$$

In addition the measurement and observation matrices $\boldsymbol{C}$ and $\boldsymbol{D}$ can be written in the following form if displacement and acceleration are to be estimated.

$$\boldsymbol{C} = \begin{bmatrix} \boldsymbol{I} & \boldsymbol{0} \\ -\boldsymbol{M}^{-1}\boldsymbol{K} & -\boldsymbol{M}^{-1}\bar{\mathbf{C}} \end{bmatrix} \quad \boldsymbol{D} = \begin{bmatrix} \boldsymbol{0} \\ \boldsymbol{M}^{-1}\boldsymbol{S}_p \end{bmatrix} \tag{10}$$

The discrete time form of the state space model is needed for the simulation and it can be obtained by

$$\boldsymbol{x}_{\boldsymbol{k+1}} = \widehat{\boldsymbol{A}}\boldsymbol{x}_{\boldsymbol{k}} + \widehat{\boldsymbol{B}}\boldsymbol{p}_{\boldsymbol{k}} \tag{11}$$

$$\boldsymbol{y}_{\boldsymbol{k}} = \widehat{\boldsymbol{C}}\boldsymbol{x}_{\boldsymbol{k}} + \widehat{\boldsymbol{D}}\boldsymbol{p}_{\boldsymbol{k}} \tag{12}$$

Where the transformed $\widehat{\boldsymbol{A}}$ and $\widehat{\boldsymbol{B}}$ matrices are

$$\widehat{\boldsymbol{A}} = e^{\boldsymbol{A}\Delta t} \tag{13}$$

$$\widehat{\boldsymbol{B}} = \left(\widehat{\boldsymbol{A}} - \boldsymbol{I}\right)\boldsymbol{A}^{-1}\boldsymbol{B} \tag{14}$$

$\widehat{\boldsymbol{C}}$ and $\widehat{\boldsymbol{D}}$ will remain the same

$$\widehat{\boldsymbol{C}} = \boldsymbol{C}, \qquad \widehat{\boldsymbol{D}} = \boldsymbol{D} \tag{15}$$

2.3 Augmented Kalman filter

The augmented Kalman filter (AKF) is a variant of the more common Kalman filter (Welch and Bishop, 2000) but they share many of the same characteristics. One similarity is that they both require three inputs: system state, process/model error covariance, and measurement noise covariance. They both work to provide a statistically optimal state estimation in the presence of uncertainties that can be from process error ($\boldsymbol{w_k}$) or measurement noise ($\boldsymbol{v}_k$). To characterize the process error and measurement noise, their covariance values are denoted by $\boldsymbol{Q}$ and $\boldsymbol{R}$, respectively. The magnitude of the matrices $\boldsymbol{Q}$ and $\boldsymbol{R}$ can be determined by the magnitude of the state vector and processing the physical measurements, i.e. sensor signal to noise ratio. Generally a constant value can be assigned to the diagonal term of these matrices. These terms discussed in more detail later in the AKF formulation.

The best starting point for the AKF is to discuss the input forces. In the case of the AKF, the input forces are unknown but they can be included in an augmented system state and estimated with the other states. The state vector is altered by the use of a random walk model. $\boldsymbol{\eta}_k$ is the noise on the derivative of the force parameter and it can be used to regularize the problem. The covariance value denoted by $\boldsymbol{S}$ is used to characterize the noise, $\boldsymbol{\eta}_k$. The equation below shows the input force, $\boldsymbol{p}_{k+1}$, with the noise added.

$$\boldsymbol{p}_{k+1} = \boldsymbol{p}_k + \boldsymbol{\eta}_k \tag{16}$$

The new state vector is shown with the superscript "*a*" representing that it has been augmented.

$$\boldsymbol{X}_k^a = \begin{Bmatrix} \boldsymbol{X}_k \\ \boldsymbol{p}_k \end{Bmatrix} \tag{17}$$

Once the new state vector is formed then the system state can be expressed in the state space model as:

$$\boldsymbol{X}_{k+1}^a = \boldsymbol{A}_a \boldsymbol{X}_k^a + \boldsymbol{\zeta}_k \tag{18}$$

$$\boldsymbol{\zeta}_k = \begin{Bmatrix} \boldsymbol{w}_k \\ \boldsymbol{\eta}_k \end{Bmatrix} \tag{19}$$

$$\boldsymbol{A}_a = \begin{bmatrix} \widehat{\boldsymbol{A}} & \widehat{\boldsymbol{B}} \\ \boldsymbol{0} & \boldsymbol{I} \end{bmatrix} \tag{20}$$

The output vector for the state space model can be written as:

$$\boldsymbol{y}_k = \boldsymbol{C}_a \boldsymbol{X}_k^a + \boldsymbol{v}_k \tag{21}$$

$$\boldsymbol{C}_a = [\boldsymbol{C} \;\; \boldsymbol{D}] \tag{22}$$

Now the measurements can be incorporated into the state space model. A general representation of how these measurements are used is shown in this simplified equation for the output vector.

$$\boldsymbol{y}(t) = \boldsymbol{S}_a \ddot{\boldsymbol{u}}(t) + \boldsymbol{S}_v \dot{\boldsymbol{u}}(t) + \boldsymbol{S}_d \boldsymbol{u}(t) + \boldsymbol{S}_s \boldsymbol{u}(t) \tag{23}$$

The matrices, $\boldsymbol{S}_a$, $\boldsymbol{S}_d$, $\boldsymbol{S}_v$, and $\boldsymbol{S}_s$, are the selection matrices for the measurements to be used in the AKF where they represent acceleration, displacement, velocity, and strain states respectively. They are a Boolean matrix showing the locations of that measurement type and have a size "$\mathbf{n_m}$ x $\mathbf{n}$" where $\mathbf{n_m}$ is the number of measurements. The strain selection matrix is the modified using the strain-displacement matrix to define its relationship to structural displacement states. The new measurement and observation matrices can be solved from Eqn. (23) excluding the strain state using:

$$\ddot{\boldsymbol{u}}(t) = -\boldsymbol{M}^{-1}\overline{\boldsymbol{C}}\,\dot{\boldsymbol{u}}(t) - \boldsymbol{M}^{-1}\boldsymbol{K}\boldsymbol{u}(t) + \boldsymbol{M}^{-1}\boldsymbol{S}_p\boldsymbol{p}(t) \tag{24}$$

Once the strain is added the complete matrices have the form shown here:

$$\boldsymbol{C} = [\,\boldsymbol{S}_s + \boldsymbol{S}_d - \boldsymbol{S}_a\boldsymbol{M}^{-1}\boldsymbol{K}\,, \boldsymbol{S}_v - \boldsymbol{S}_a\boldsymbol{M}^{-1}\overline{\boldsymbol{C}}\,\,], \quad \mathbf{D} = \left[\boldsymbol{S}_a\boldsymbol{M}^{-1}\boldsymbol{S}_p\right] \tag{25}$$

Similar to the Kalman filter, the AKF also uses two major steps; time update or *a priori* step, and measurement update, also known as the *a posteriori* step. The time update contains the *a priori* error covariance matrix, $\boldsymbol{P}_{k|k}$, hence the name *a priori* step. The measurement update makes use of the Kalman gain, $\boldsymbol{L}_k$, and the *a posteriori* error covariance matrix, $\boldsymbol{P}_{k+1|k}$, hence the name *a posteriori* step. These two steps are shown here.

Time update:

$$\widehat{\boldsymbol{X}}^a_{k|k-1} = \boldsymbol{A}_a\widehat{\boldsymbol{X}}^a_{k-1|ko} \tag{26}$$

$$\boldsymbol{P}_{k|k-1} = \boldsymbol{A}_a\,\boldsymbol{P}_{k-1|ko}\boldsymbol{A}_a^T + \boldsymbol{Q}_a$$

Measurement update:

$$\boldsymbol{L}_k = \boldsymbol{P}_{k|k-1}\boldsymbol{C}_a^T\left(\boldsymbol{C}_a\boldsymbol{P}_{k|k-1}\boldsymbol{C}_a^T + \boldsymbol{R}\,\right)^{-1} \tag{27}$$

$$\widehat{\boldsymbol{X}}^a_{k|k} = \widehat{\boldsymbol{X}}^a_{k|k-1} + \boldsymbol{L}_k(\boldsymbol{y}_k - \boldsymbol{C}_a\widehat{\boldsymbol{X}}^a_{k|k-1})$$

$$\boldsymbol{P}_{k|k} = \boldsymbol{P}_{k|k-1} - \boldsymbol{L}_k\boldsymbol{C}_a\boldsymbol{P}_{k|k-1}$$

$\boldsymbol{Q}_a$ is an augmented matrix defined by $\boldsymbol{Q}$ and $\boldsymbol{S}$ which are the covariance matrices for the process error and noise in the force input, respectively. The form of $\boldsymbol{Q}_a$ is given below.

$$\boldsymbol{Q}_a = \begin{bmatrix}\boldsymbol{Q} & \mathbf{0}\\ \mathbf{0} & \boldsymbol{S}\end{bmatrix} \tag{28}$$

For the deployment of the AKF in the field it is necessary to determine the different covariance matrices values, for simulations this process can be done using trial and error to find the best values, unlike the field application of the filter where determining these covariance values is difficult. However, there are methods used in practice and the determination of the measurement error covariance, $\boldsymbol{R}$, is possible since this will be measured and off-line samples can be used to calculate the variance values. The covariance values for the process error is more difficult to obtain since the process is not observed directly but rather this process is to be estimated. A common approach to overcome this challenge is to, first, assume a poor process model by adding uncertainty to the process via the covariance values of $\boldsymbol{Q}$ and, secondly, tuning of the filter parameters can be done off-line by using a system identification process.

In summary, the below flow chart shows the augmented Kalman filtering process for a single time step along with a simplified description of each step.

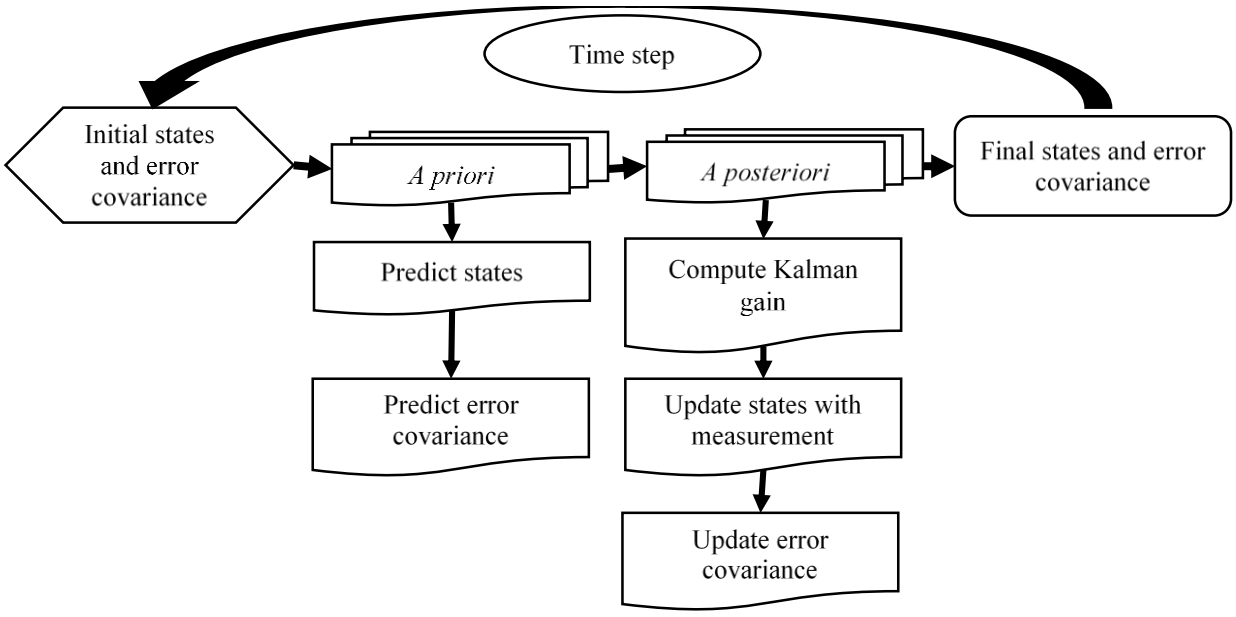

Figure 4: Kalman filter process for single time step

Starting on the left of the process, some initial states and error covariance matrices are input into the system; these initial values for the first time step do not need to be very accurate since the filter will self-correct after a short burn-in period. This initialization step is followed by the prediction, *a priori* step. For this step, the newly predicted states are estimated using the numerical model and *a priori* estimate error covariance matrix is constructed. Following the prediction is the correction, *a posteriori* step, where the Kalman gain is calculated, which to put simply is the weighting factor for the measurement update. After the Kalman gain is calculated then the estimated states are "corrected" using the new information from the measurements to get the final estimated states. Finally, the estimate error covariance matrix is updated before it and the final estimated states are passed onto the next time step to be used as the input.

3 Numerical validation

In this section, there are 5 separate simulations ran to investigate the accuracy given by AKF for strain estimation and factors that may influence the strain estimation. To begin with, the various properties of the plate that was modeled are introduced. The dimensions were set as 40.64 cm (16 inches) by 30.48 cm (12 inches) by 0.3175 cm (1/8 inches) thick. The other required material properties were set to model A36 steel. Young's modulus equal to $200x10^9$ Pa and the density set as 7800 kg/m^3. A Poisson's ratio of 0.3 was used. Modal damping of 1% is considered in the plate. The time step for the simulation is taken to be 1/2000. The plate is cantilevered by having one of the longer, i.e. 40.64 cm, sides fixed and the other three sides free. These boundary conditions are similar to a possible setup that would be used for a gusset plate in a building. Additionally, to make the simulations as realistic to field conditions as possible a modeling error is introduced in the system by varying the Young's modulus. Measurement noise is also instilled by adding contamination to the sensor data.

The plate was discretized with a 10 x 10 mesh of quadrilateral elements. The figure below shows the meshing with the global numbering of the nodes.

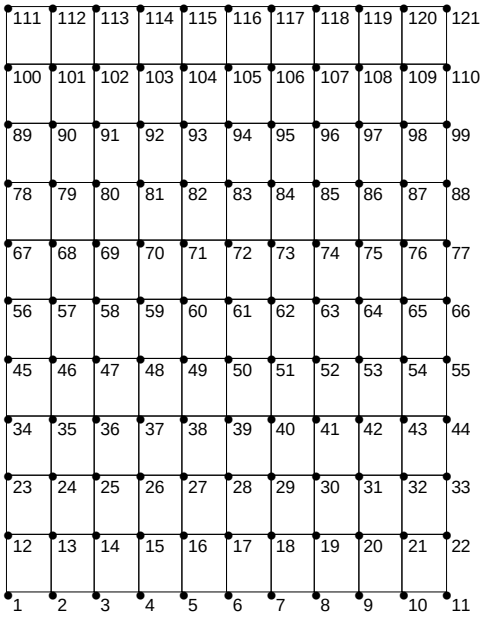

Figure 5: 10 x 10 mesh with global node numbering for the plate

The plate is then excited by two non-zero mean excitations that are applied simultaneously in opposite directions and perpendicular to the plate at the corners opposite to the fixed end as shown below.

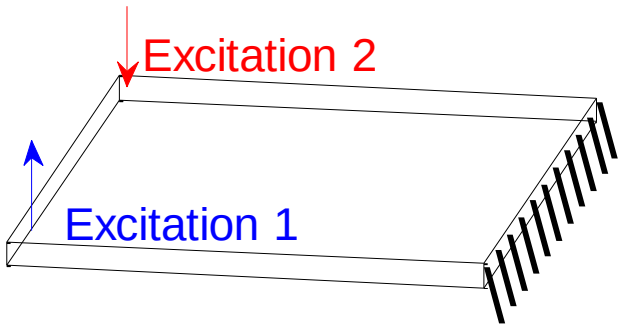

Figure 6: Cantilever plate with excitation locations

The applied excitations are chosen to represent a realistic and complicated loading scenario. Excitation 1 is a ramping force that starts at 1 second and reaching a maximum force of 89 N (20 lb-ft) at 5 seconds with bandlimited white noise added. Excitation 2 is a low frequency varying

(half sine wave function) excitation with bandlimited white noise added. Excitation 2 starts at zero then increases to a maximum force of 44.5 N (10 lb-f) before decaying back to zero. The time history of the input excitations are shown in the figure below.

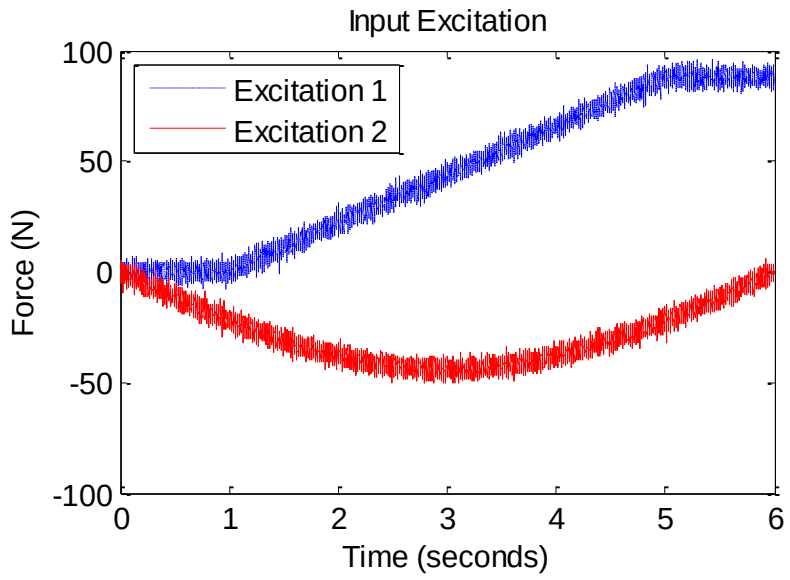

Figure 7: Excitation 1 (ramping force) and Excitation 1 (low frequency force)

The excitations were then applied to the state space model to generate the structural responses, i.e. displacement and acceleration, and the strain values were also calculated from the strain-displacement relationship. An example strain time history response for the strain components, ε_x, ε_y, and γ_{xy}, at node 70 is shown below. This gives an indication of how the strain histories should appear when responding to the input excitation.

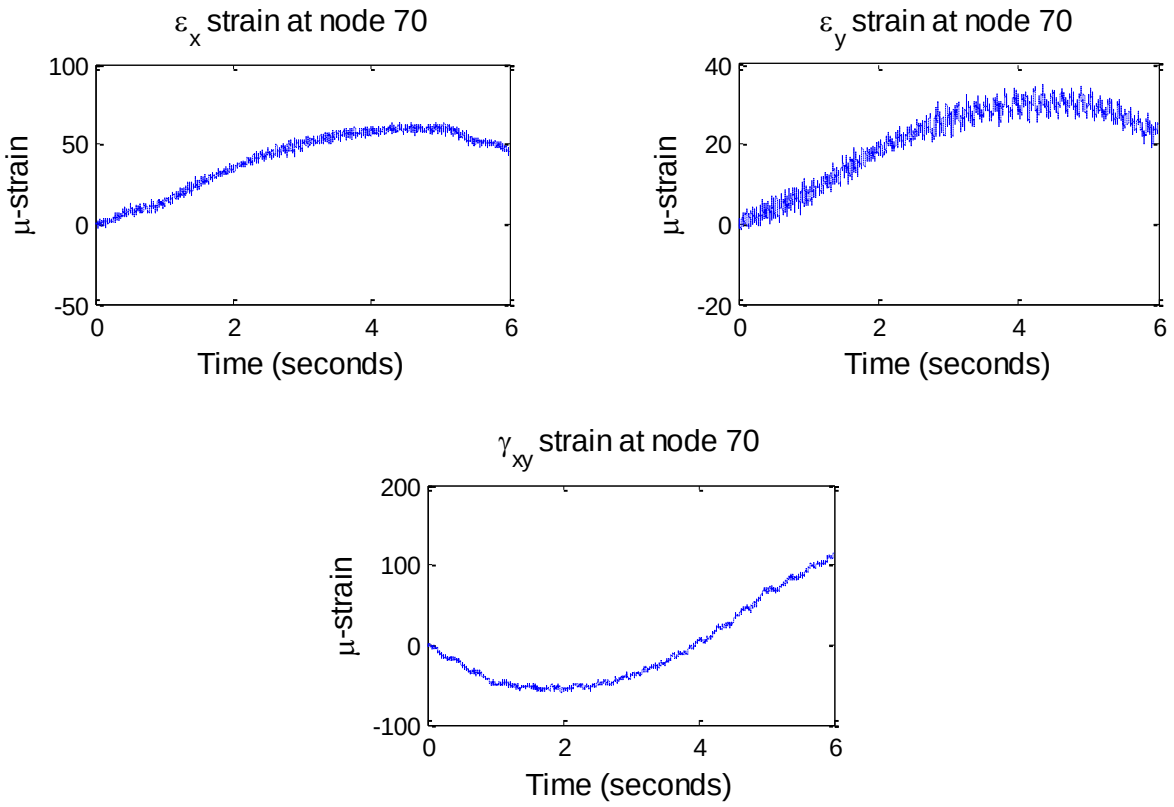

Figure 8: Complete strain history for all strain components at node 70

The above steps are necessary to derive the simulated measurement data. Then from the complete data it is possible to taken simulated measurements from a few select locations and use it as the input into the AKF. Since this work was done prior to the development of a sensor optimization scheme the cases in this section had the measurement locations chosen through experience and a trial and error process. For an accurate comparison it was necessary to keep the locations of the measurements the same between the different cases so that the measurement locations would not become a factor that would influence the strain estimation result. The performance of the AKF's strain estimation can be evaluated by calculating the error between the estimated and reference strain values using the equation below.

$$Error = \frac{\sqrt{\Sigma\left(\boldsymbol{\varepsilon}_{est} - \boldsymbol{\varepsilon}_{ref}\right)^2}}{Signal\ length} \tag{29}$$

Where $\boldsymbol{\varepsilon}_{est}$is the estimated strain values from the filter and $\boldsymbol{\varepsilon}_{ref}$ is the reference values.

To show the performance of the AKF's strain estimations when different types of measurements are used as the input there are three cases investigated. As mentioned before benefits of using reference-free measurements made strain and acceleration measurements the types of measurements to be studied. The first two cases show the effect of using a single type of sensor as the input for the AKF. The third case shows the effect of using multi-metric data for the input. This final multi-metric case is also subdivided into four cases to compare the effect that measurement noise and modeling error has on the system. The three cases are summarized below.

Case 1)

- Three acceleration only measurements are used
- 5% Modeling error and 2% measurement noise is considered

Case 2)

- Three strain only measurements are used
- 5% Modeling error and 2% measurement noise is considered

Case 3)

- One acceleration and two strain measurements (multi-metric) used together

- Four subcases are used to compare the effects of 5% modeling error and 2% measurement noise
- Then the multi-metric results are compared with Case 1 and Case 2

Case 1: Acceleration only

Case 1 considers the use of acceleration measurements only as the input to the AKF. The AKF formulation will then change so that the measurement and observability matrices have the form shown here.

$$\boldsymbol{C} = [\, -\boldsymbol{S}_a\boldsymbol{M}^{-1}\boldsymbol{K}\,, -\boldsymbol{S}_a\boldsymbol{M}^{-1}\overline{\boldsymbol{C}}\,\,], \mathbf{D} = \left[\boldsymbol{S}_a\boldsymbol{M}^{-1}\boldsymbol{S}_p\right] \tag{6}$$

The selection matrix, $\boldsymbol{S}_a$, is modified so the location of the acceleration measurements are selected for the nodes where the sensors are to be placed. The placement of the accelerometers are at nodes 12, 58, and 100 as shown below.

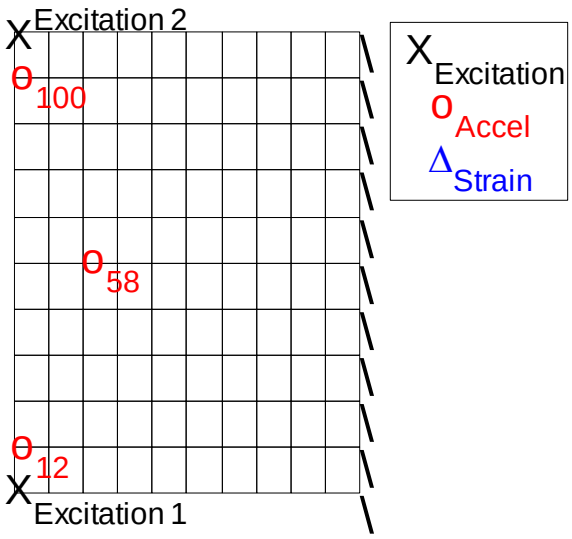

Figure 9: Acceleration measurement locations

It can be noted that the acceleration data at these nodes was taken to only measure the acceleration of the out-of-plane motion, $\ddot{w}$, and not the rotation acceleration i.e. $\ddot{\theta}_x$ and $\ddot{\theta}_y$. Using acceleration measurements as the only input for the AKF the response of the plate at all of its dofs can be estimated and the response is used to calculate the strain components. Here the strain history is shown at the unmeasured location, node 1, for shear strain component, γ_{xy}.

a. **b.**

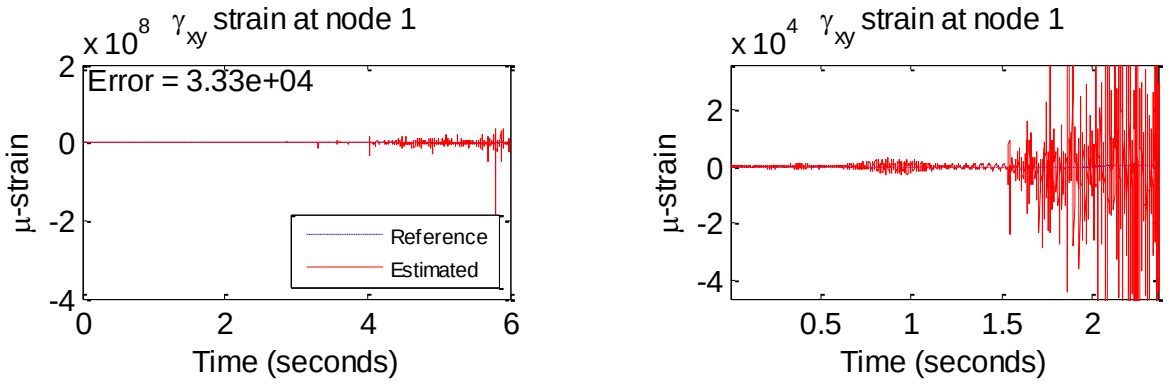

Figure 10: Complete, (a) and detail, (b), strain history estimation using acceleration measurements only with model error (5%) and measurement noise (2%)

It is seen that there is an instability in the formulation as the estimation diverges and the result is similar for the other strain components. This phenomenon has been reported in several papers and is due to the process being unobservable. (Lourens et al., 2012, Naets et al., 2015) It is also understood that the addition of noise in the measurements and error in the processe make the response estimation from acceleration measurements generally unstable. However the use of acceleration measurement is good at giving information about the system on a global level as shown later. As considered here, the acceleration measurements alone are not sufficient and attempting to increase the number of acceleration sensors does not solve the instability issue.

Case 2: Strain only

Case 2 considers the use of strain measurements only as the input to the AKF. The AKF formulation will then change so that the measurement and observability matrices have the form shown here.

$$\boldsymbol{C} = [\boldsymbol{S}_s\,, \mathbf{0}]\ \mathbf{D} = [\mathbf{0}] \tag{6}$$

The selection matrix is modified so the location of the strain measurements are selected. The placement of the strain sensors are at nodes 2, 58, and 100 as shown in the figure below. The use of the subscript for the strain measurements in sensor location figures denote the strain component measured, e.g. XY indicate that the shear strain was measured at the node.

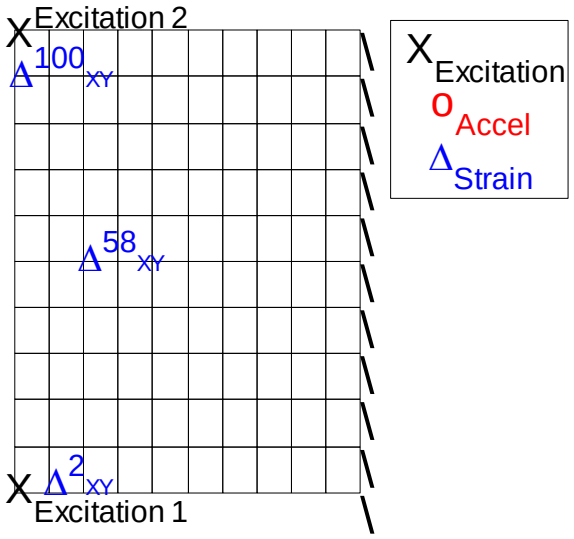

Figure 11: Strain measurement locations

Using the AKF algorithm with three strain measurements as the input, the filter is ran to estimate the states and associated strain values of the plate at all of its nodes. The figure, shown below, has the average strain error calculated using Eqn. 29 for all 363 strain components and the average was taken of the error for the 363 strain components to obtain a single error term for easy comparison.

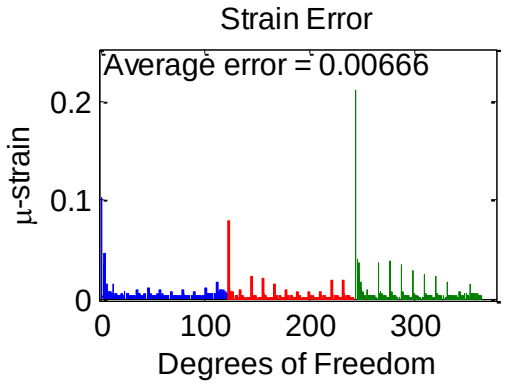

Figure 12: Error shown at all strain components for strain measurements only with model error (5%) and measurement noise (2%)

In the previous figure, the dofs from 1 to 121 correspond to the x-direction component of the strain, ε_x, for nodes 1 to 121. Similarly, the dofs 122 to 242 are the y-direction component of the strain,

ε_y, for nodes 1 to 121 and likewise, dofs 243 to 363 correspond to the shear strain component, γ_{xy}, for nodes 1 to 121.

The total average error, found by taking a simple average of the individual strain errors, can give a measure of error for the entire plate. The average strain error for this case is found to be 0.00666 micro-strain. The figures below show the strain history and error value for the strain component, ε_x, at node 70 and for the shear strain component, γ_{xy}, at node 1 along with a corresponding detailed view for a shorter time interval.

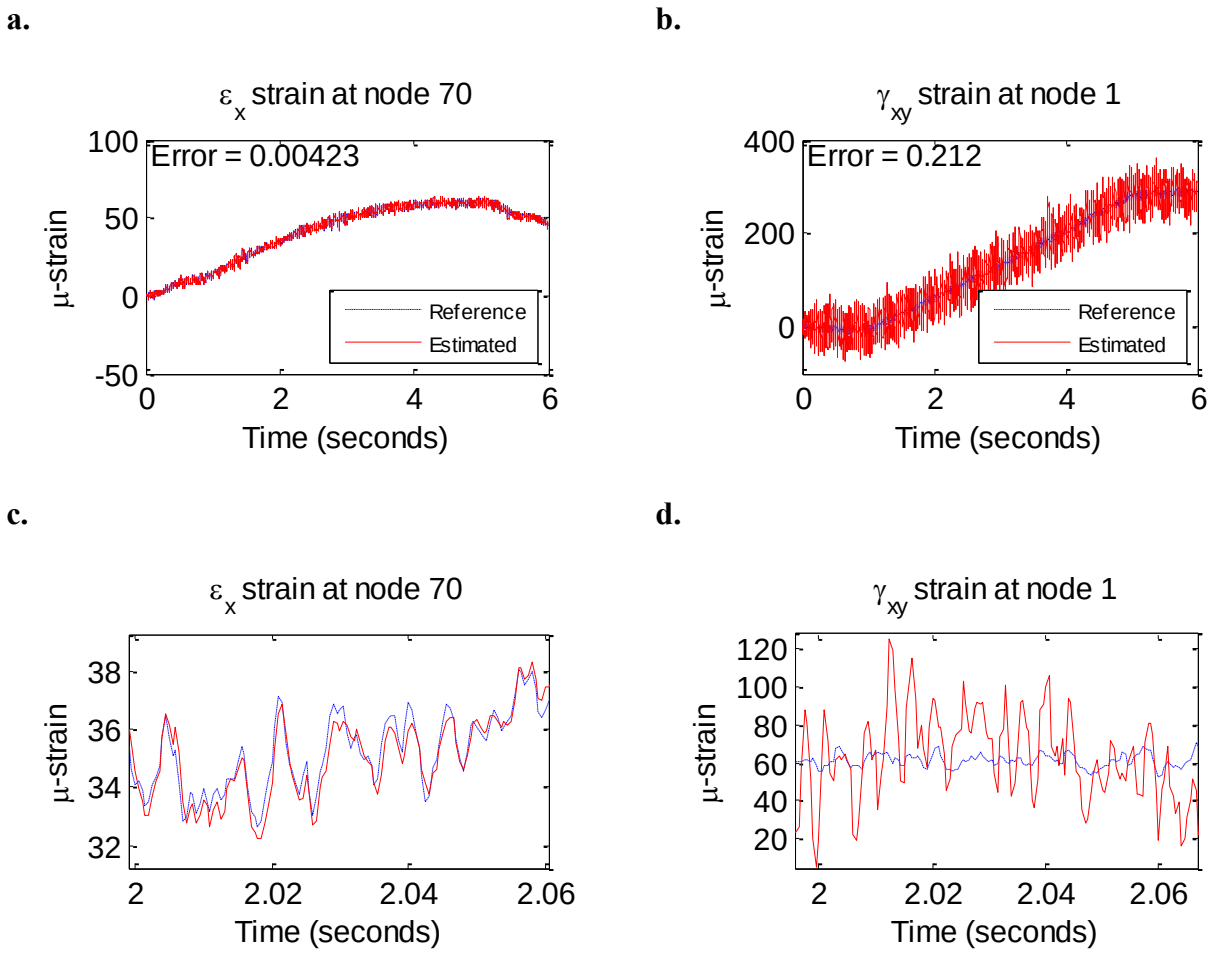

Figure 13: Complete, (a) (b), and detail, (c) (d), of the strain history shown for the strain measurements only with model error (5%) and measurement noise (2%)

The strain estimation at the majority of the nodes is good but estimation around the excitation locations is not as accurate. This inaccuracy shown in Figure 12.b where it shows the estimated strain catching the low frequency change but the error value is 30 times the average error value. From the detailed view, Figure 12.d, the error between the estimated and reference strain values can clearly be seen. The estimated strain is able to capture the overall ramping force but the high frequency dynamic response is not captured well.

Using the frequency response it is easy to show the difference of the reference and estimated values in the frequency domain. In the figure below the response matches in the lower frequency but for higher frequency it does not give good results.

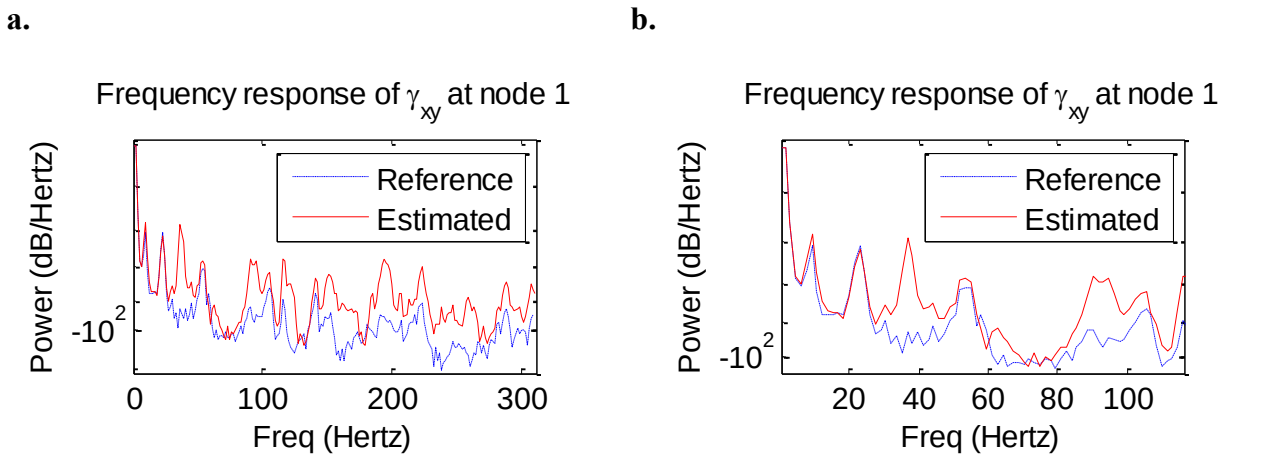

Figure 14: Complete (a) and detail (b) of the frequency response shown for the strain measurements only with model error (5%) and measurement noise (2%)

From the results, the conclusion is that using strain measurements only as an input to the AKF can provide good results in capturing the overall trend of the strain changes, i.e. low frequency response, but it does not perform well for high frequency response of the structure.

Case 3: Acceleration and strain

Using the multi-metric measurements, acceleration and strain, the AKF formulation is changed by modifying the measurement and observability matrices to the following form.

$$\boldsymbol{C} = [\, \boldsymbol{S}_s - \boldsymbol{S}_a \boldsymbol{M}^{-1} \boldsymbol{K} \,, -\boldsymbol{S}_a \boldsymbol{M}^{-1} \overline{\boldsymbol{C}} \,] \; \mathbf{D} = \left[\boldsymbol{S}_a \boldsymbol{M}^{-1} \boldsymbol{S}_p \right] \tag{6}$$

The selection matrix is modified so that two shear strain measurements at nodes 2 and 100 and one acceleration measurement at node 12 are used as the input. The locations of sensors are shown in the figure.

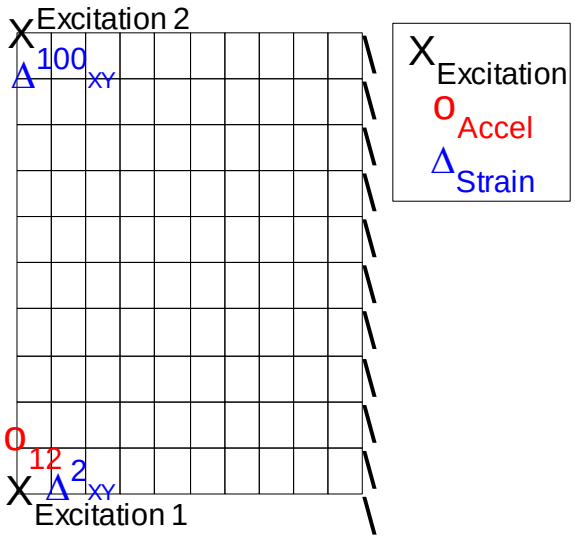

Figure 15: Acceleration and strain measurement locations

For the multi-metric measurement case a comparison is made between four different cases. This comparison shows the sensitivity of the AKF to the presence of measurement noise and modeling error. Then the multi-metric results are evaluated against the strain measurement only case.

Case 3.a

- No modeling error and no measurement noise

Case 3.b

- 2% measurement noise included and no modeling error

Case 3.c

- 5% modeling error included and no measurement noise

Case 3.d

- 5% modeling error and 2% measurement noise included

Four simulations are ran for the cases and the figure below shows the strain error plots for the four cases.

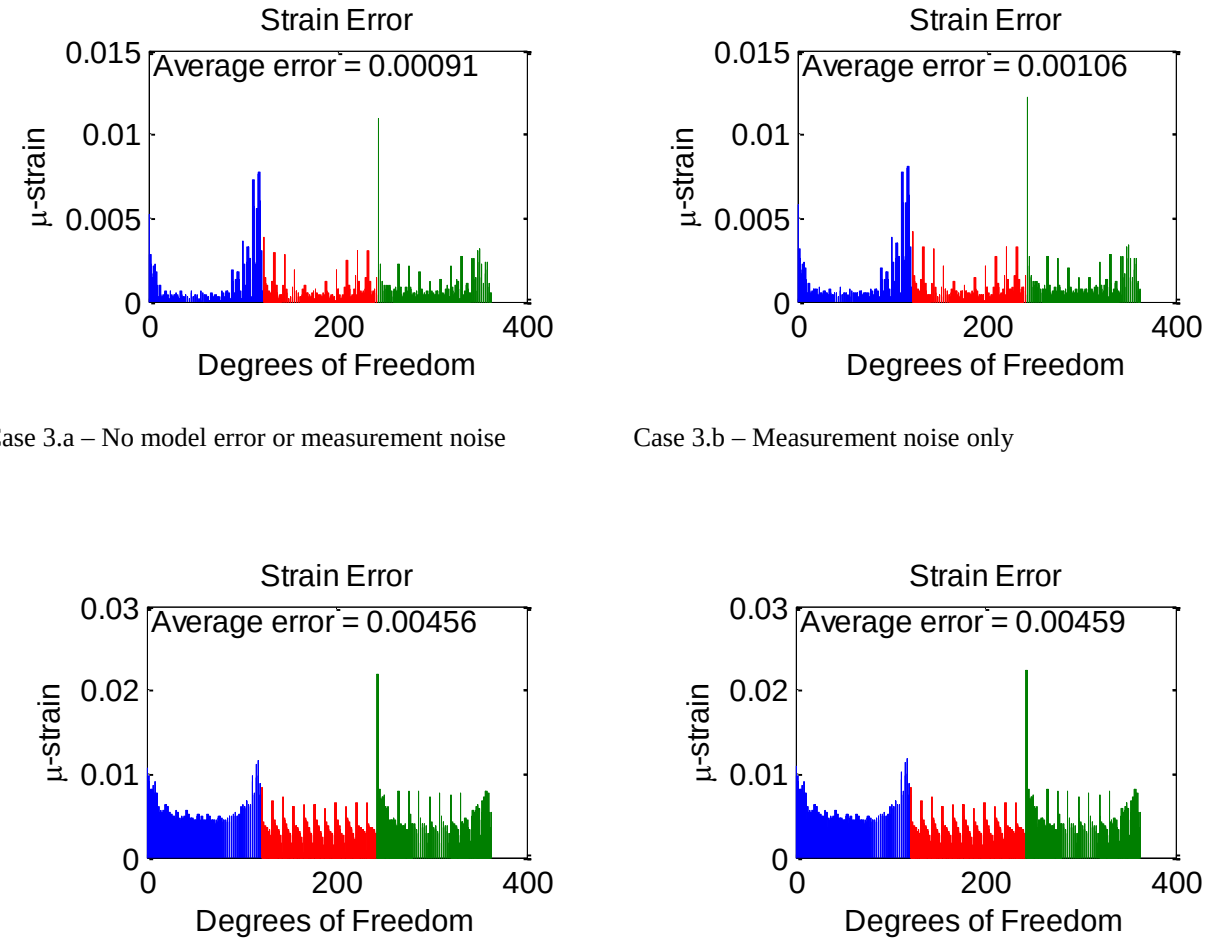

Case 3.a – No model error or measurement noise

Case 3.b – Measurement noise only

Case 3.c – Model error only

Case 3.d – Model error and measurement noise

Figure 16: Error shown at all strain components for multi-metric measurements

From the above figures, a few conclusions can be made about the effect of model error and measurement noise on the AKF results. Comparing Case3.a to Case 3.b, it is seen that the effect of the measurement noise is minimal. This can be attributed to two reasons; the first, the filter considers this noise and, secondly, the filter is able to use the system model to estimate the strain

values accurately. The comparison Case 3.a and 3.c shows that the effect of model error is more substantial and causes more error in all the estimated strain components. This is expected since the unmeasured location are more numerous than measured locations and estimation of the unmeasured location will depend on the model. However, the AKF can still provide accurate estimates of the strain given its robust formulation where model error is accounted for. In addition, it is feasible to place an increased number of sensors if more accuracy is needed.

Now, Case 3.d is the case of the greatest interest and it is where the highest strain error occurs out of the four subcases. This is because Case 3.d has both model error and measurement noise but this case is to be compared with the strain measurement only case which also had model error and measurement noise included. Looking at the average strain error, it is found to have decreased from 0.00666 micro-strain for the strain measurement only case to 0.00459 micro-strain for the multi-metric case. This shows that the overall accuracy increased while using multi-metric data as input to the AKF. The figure below shows the strain history and error values for the strain component, ε_x, at node 70 and for the shear strain component, γ_{xy}, at node 1 along with corresponding detailed views.

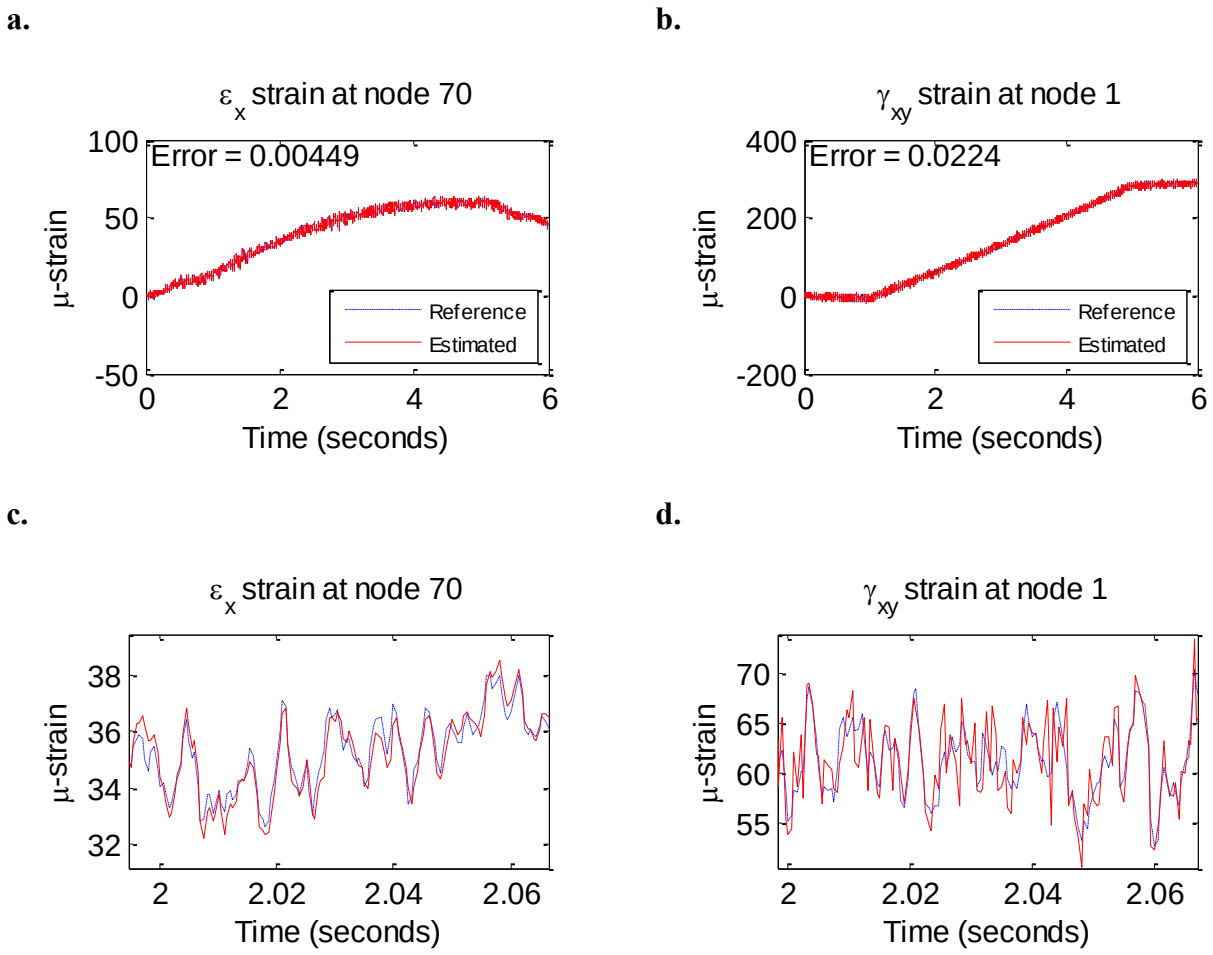

Figure 17: Complete, (a) (b), and detail, (c) (d), of the strain history shown for the Case 3.d; model error (5%) and measurement noise (2%)

Now considering the strain history plots and, in particular, Figure 7.d, the detailed view for γ_{xy} at node 1, it is shown that the estimated and reference strain are closely matching. The γ_{xy} at node 1 has a significant reduction of two orders of magnitude in the error value when compared to the case using only strain measurements as the input to the AKF.

The comparison of strain measurement only case versus multi-metric case can also be made in the frequency domain. Looking at the structure's frequency response it shows the reference and estimated values match very well for the multi-metric case, this is in contrast to the frequency

response using strain measurement only. The figure below shows the frequency response now matching in the high frequency and low frequency.

a. **b.**

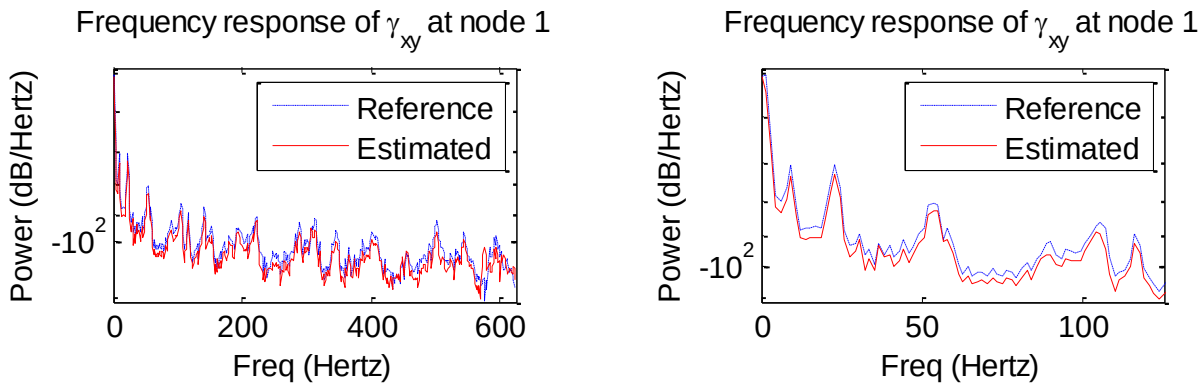

Figure 18: Complete (a) and detail (b) of the frequency response shown for the Case 3.d with model error (5%) and measurement noise (2%)

Based on the simulation results, it is concluded that the effect of measurement noise is minimal when compared to the effect of model error on strain estimation by the AKF. However, the best practice would be to minimize the effect of both and the proper tuning of the filter parameters can help to accomplish this. The important conclusion that can be made from this case is that the combination of acceleration and strain measurements, i.e. multi-metric, as an input to the AKF can provide very accurate results for strain estimation at all the nodes and for all their strain components. Multi-metric input provides better results than the strain measurement only case and it captures all of the strain changes, i.e. low frequency response and high frequency response.

Case 4: Arbitrary sensor placement

The next case is to test the sensitivity of the strain estimation to the placement of the sensors. It is logical to predict that changing the sensor locations will have an effect on the strain estimation.

Previous work has studied the effect of the sensor placement and found the placement closer to the excitation location is better. (Naets et al., 2015, Ghajari et al, 2013) To demonstrate the severity that improper sensor placement can have, the sensor placement is arbitrarily changed. The input to the AKF once again consisted three total sensors where there are two strain measurements; ε_y is measured at node 23 and ε_x is measured at node 103, and one acceleration measurement is measured at node 2. The figure below shows the arbitrary sensor layout.

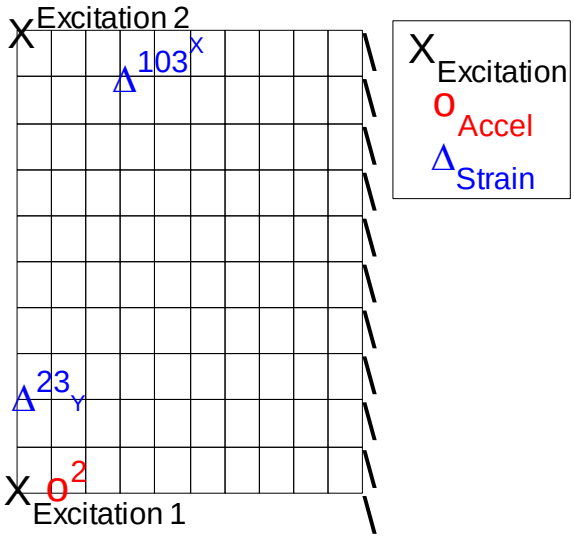

Figure 19: Acceleration and strain measurement locations (arbitrary placement)

For this layout, measurement noise and modeling error is once again considered as 2% and 5%, respectively, to have an equal comparison with the previous results. It can be seen strain error figure, shown below, that the average error of the strain estimation increases by a factor of 1000 with the largest error values occurring around the location of Excitation 2, i.e. node 111.

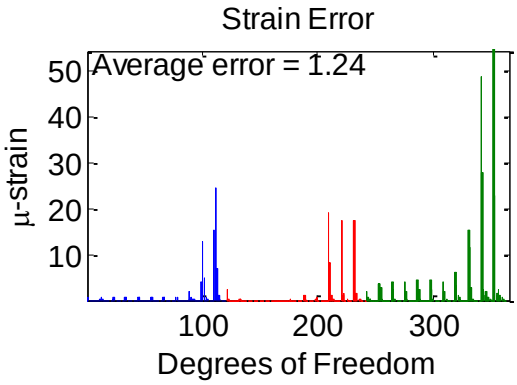

Figure 20: Error shown at all strain components for the arbitrary sensor placement

The increase in strain estimation error can be shown in the strain history the γ_{xy} strain component at node 1, and the ε_x strain component at node 70. In the figure below, it is seen that the strain estimation of both components have problems with the high frequency response and this makes it difficult to understand the low frequency component which deteriorates for the whole estimated strain history.

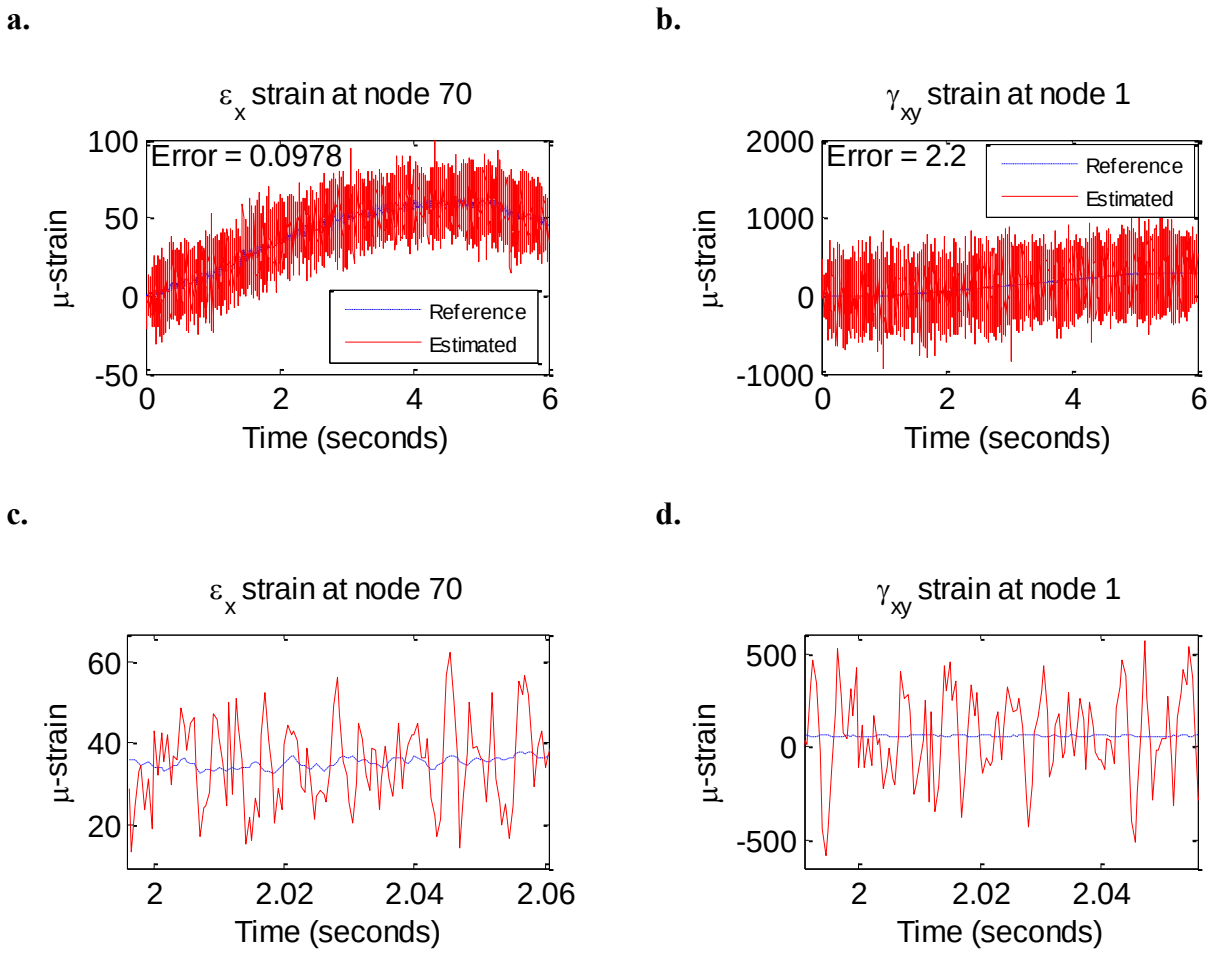

Figure 21: Complete, (a) (b), and detail, (c) (d), of the strain history for the arbitrary sensor placement

It is useful to look at the frequency domain to get an understanding of the severity of the problem created from an arbitrary sensor placement. The frequency response shows the decrease in accuracy with only one peak, the forcing frequency of the half sine wave, being caught by the estimated values. The figure below is the frequency response at node 1.

a. **b.**

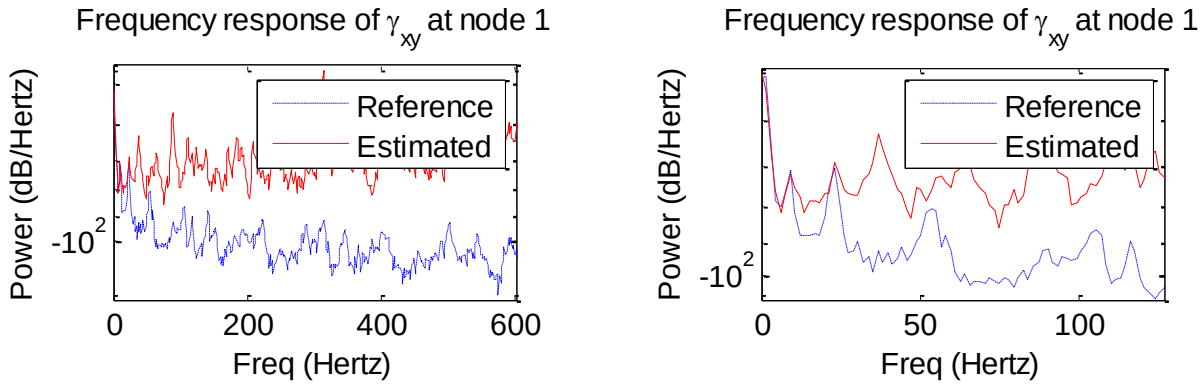

Figure 22: Complete (a) and detail (b) of the frequency response shown for the arbitrary sensor placement

The key conclusion to make from this case is that the AKF's performance is not just a function of the type or number of measurements to be used as an input but it relies heavily on the placement of the sensors. The input to the filter should as a minimum be able to provide information about the excitations since it is possible to use the model to estimate the other states if these states are sufficiently accurate. This idea of placing sensors near the excitation locations was cited before but it does not provide a complete solution about optimal sensor placement. The next case considers how the structural characteristics relate to the filter's input.

Case 5: Flexible plate structure

In this case, the structure is altered so that its first natural frequency is decreased and the structure can then be termed a low frequency structure. Previously, the plate structure had a first natural frequency of 28.9 Hz and now the first natural frequency will be decreased by increasing the dimensions from a width of 30.48 cm (12 inch) to 182.88 cm (72 inch) and from a length of 40.64 cm (16 inch) to 60.96 cm (24 inch). The thickness is also decreased from 0.3175 cm (1/4 inch) to

0.0396 cm (1/64 inch). The result of these changes make the plate more flexible and the new first natural frequency value is calculated to be 0.14 Hz. Though new dimensions of the plate are not realistic for civil applications these changes allow a low frequency structure to be investigated and can help to better understand the AKF. All other properties, i.e. Young's modulus, density, Poisson's ratio, and modal damping, remain the same as previous simulations. Once again 5% modeling error and 2% measurement noise are included.

The location of the input excitations was kept the same but the magnitude needed to be decreased to keep the response in the elastic range. Excitation 1 is an identical ramping force, as previously used, but the maximum force value is decreased to 0.089 N (0.02 lb-ft) before bandlimited white noise added. Once again, Excitation 2 is a low frequency varying (half sine wave function) excitation with a maximum force of 0.0667 N (0.015 lb-f) before bandlimited white noise is added. The input excitations are shown in figure below.

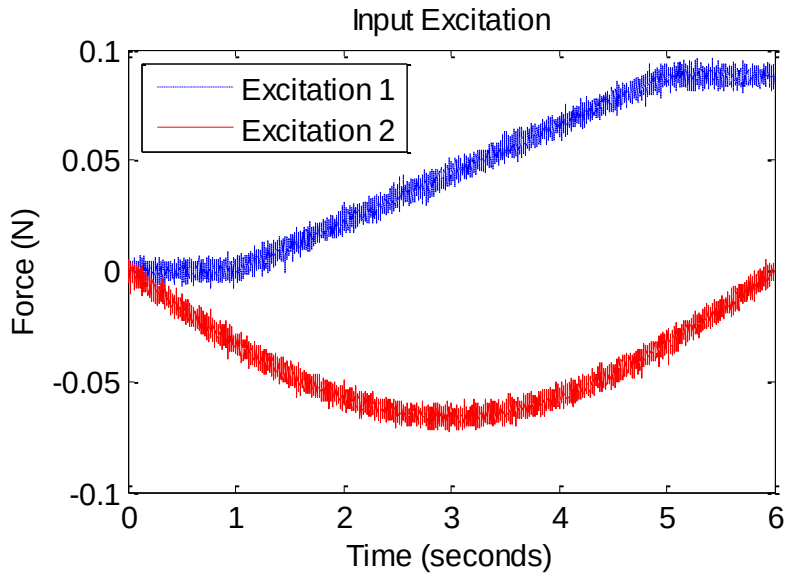

Figure 23: Excitation 1 (ramping force) and Excitation 1 (low frequency force)

Using the flexible case, four subcases are compared. This comparison shows how the different structural characteristics of the flexible plate effect the required input to the AKF, in particular the type and number of measurements.

Case 5.a

- Three strain measurements
- Identical sensor type, number, and placement as Case 2

Case 5.b

- Two strain measurements and one acceleration measurement
- Identical sensor type, number, and placement as Case 3.d

Case 5.c

- One strain measurement and one acceleration measurement
- Number of total measurements reduced to two

Case 5.d

- Two strain measurements
- Number of total measurements reduced to two

The figure below shows the strain error for the four subcases.

a.

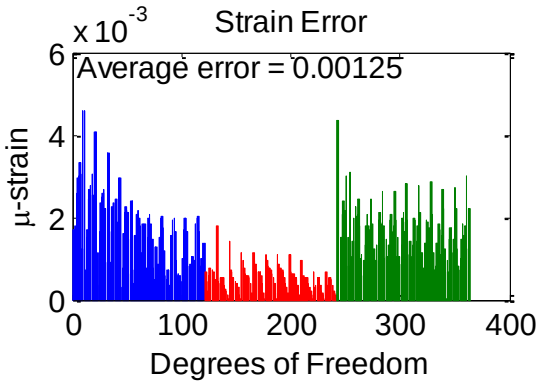

Case 5.a – Two strain measurement and one acceleration measurement

b.

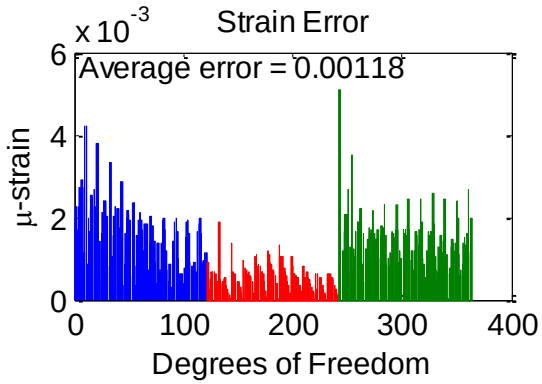

Case 5.b – Three strain measurement

c.

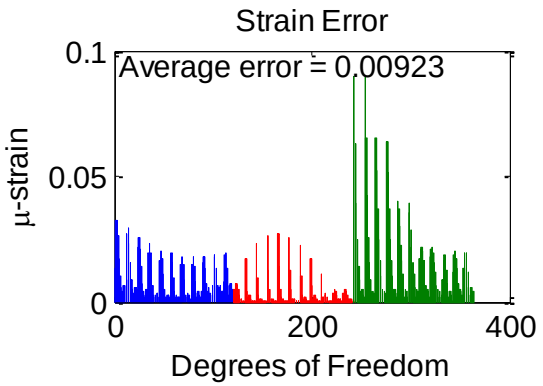

Case 5.c – One strain measurement and one acceleration measurements

d.

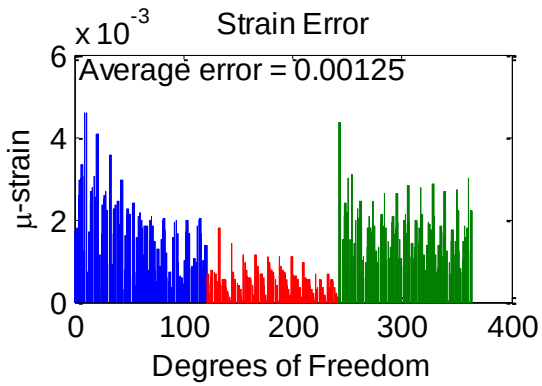

Case 5.d – Two strain measurement

Figure 24: Error shown at all strain components for flexible plate

There is no noticeable difference in the average strain error, i.e. 0.00125 micro-strain for the two strain and one acceleration measurements versus 0.00118 micro-strain for the three strain measurements, between the first two cases where three sensors are used. This is the comparison using the previous sensor placements but for the flexible plate. This result is interesting because it

is expected that since the structure has a low frequency response then using the strain measurements only should be sufficient to capture it.

However, if Case 5.c and 5.d are considered where the number of sensors is reduced to two sensors total then it gives some insight into the results. First, Case 5.c is discussed. The figure below shows the sensor placement where one strain measurement and one acceleration measurement is used as input.

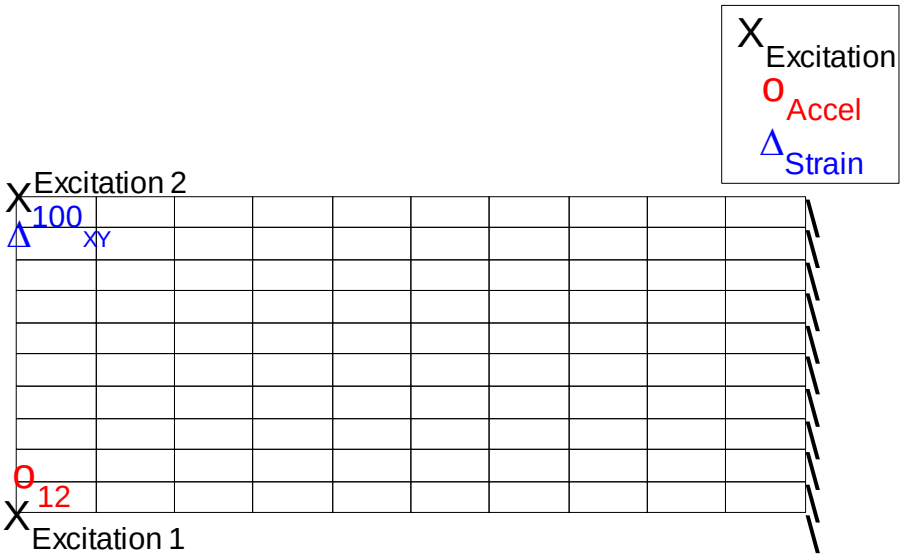

Figure 25: One strain and one acceleration measurement locations (Reduced number of measurements)

From Figure 22.c, the average strain error value is 0.00923 micro-strain for this sensor layout which is the largest error value from all of the four subcases. To understand how bad the result is the strain history for the γ_{xy} strain component for node 1 is shown below.

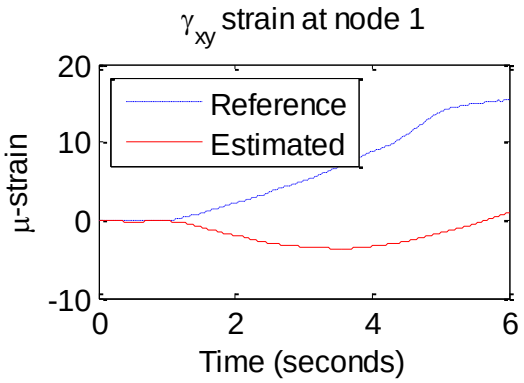

Figure 26: Complete strain history shown for the Case 5.c

It is seen that the estimated and reference strain values do not match and this two sensor placement is inaccurate. Now, if this is compared with Case 5.d where two strain measurement are used with their placement shown in the below figure.

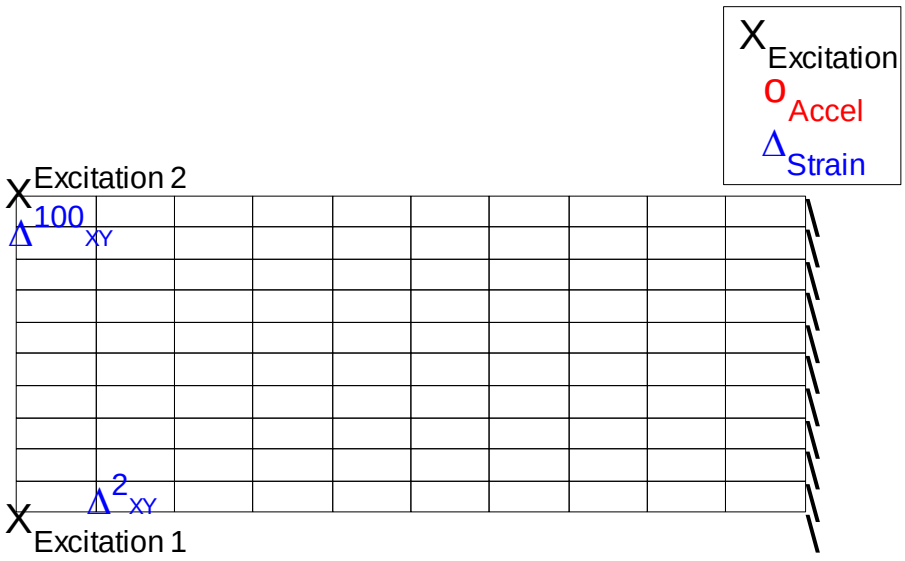

Figure 27: Two strain measurement locations (Reduced number of measurements)

For Case 5.d, it has an average strain error value 0.00125 and if the strain history for the γ_{xy} strain component for node 1 is considered the accuracy of the strain estimation is seen to match well with the reference values. The figure below shows this strain history.

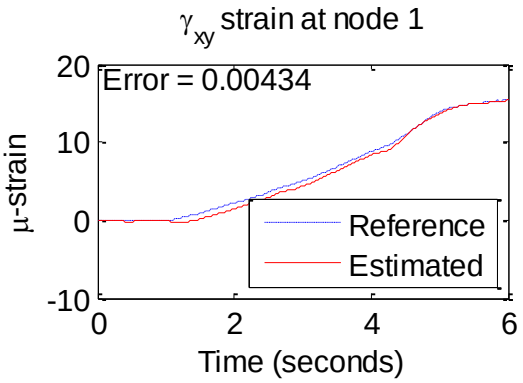

Figure 28: Complete strain history shown for the Case 5.d

When these four subcases are considered together there are a few key conclusions that can be made. It is seen that Case 5.a, b, and d produce similar average strain error values while Case 5.c gives a higher average strain error. This means that for a lower frequency structure it is not necessary to have as many sensors placed on the structure since the reduction from three sensors to two sensors can provide equally accurate results. This is with the caveat that the two sensors are able to provide relevant information to the structural response. To determine what sensor is providing the more relevant information the structural characteristics are considered.

In the case of a low frequency structure, it is clear that strain measurements will provide more pertinent information as opposed to acceleration measurements. The low frequency structure does not have a lot of high frequency response since the structure acts as a low-pass filter to the input excitations. This filtering effect is shown in the below figure of the displacement response in the out-of-plane, w, direction at node 1 and it is clear that the high frequency component from the excitation is no longer present.

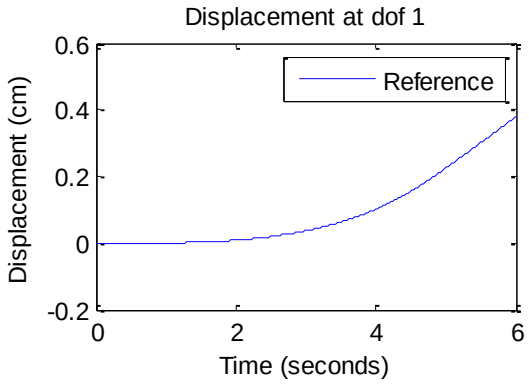

Figure 29: Complete displacement history at node 1 for the flexible plate

The figure above shows the low-pass filtering that the flexible structure provides and this affect decreases the significance of the information given from the acceleration measurements since the acceleration values will be very small.

From this case, the following conclusions are made; first, changes in the structural characteristics have a significant effect on the required input to the AKF. The affect may change the type and number of measurements, this happened for the flexible plate used here. Secondly, for low frequency structures the strain measurement information provides more valuable information than the acceleration measurement information. Therefore, the strain measurement are the preferred input to the AKF. The implications of this are that the multi-metric measurements will not always give the best results and careful consideration of the structural characteristics is needed. Finally, when the structural response slowly varies meaning the response is less dynamic, as with a flexible plate, the number of measurements that are needed to get accurate results from the AKF is reduced.

3.1 Summary

The results of the numerical simulations show that the use of the AKF for estimating strain at all locations of the plate, i.e. all nodes, is accurate. These results are in the presence of measurement noise and model error. Furthermore, there are multiple input excitations which have non-zero mean values and include bandlimited white noise making the applied excitations more realistic. From the first three cases, it is shown that the use of a multi-metric, i.e. strain and acceleration measurements, as the input into the AKF produces the best results of strain estimation at all locations including unmeasured locations. This multi-metric approach outperforms a strain measurement only approach and using the acceleration measurement only approach is unstable.

Next, the effect of the measurement noise and model error on the strain estimation is considered in subcases of the third simulation and it is concluded that the model error has more significant effect because the filter uses the model to estimate strain at unmeasured locations. These unmeasured locations are obviously more widespread than the measured ones making the error more widespread. It is noted that proper tuning of the filter can minimize this error and the filter has a parameter that accounts for the model error. Also, the number of input measurements can be increased to gain more accuracy if needed.

Finally, Case 4 and 5 show the importance of the input to the AKF. Specifically in Case 4 where the use of an arbitrary sensor placement gives higher strain error. This means the location of the sensors should be as near to the input excitation to provide the best results this is in agreement with previous work. This is the most basic way to address the challenge of sensor placement but it is not the only or even the best solution as will be discussed in the next section. Case 5, where the flexible plate is used, demonstrates that each structure will be unique but also a few guidelines can

be followed to get the best results. One guideline is that the structural response characteristics are key to understand and a low frequency structure versus high frequency structure is an important distinction to make. A low frequency acts like a low-pass filter and the use of strain measurements only as the input to the AKF can provide an accurate strain estimation as opposed to multi-metric input. Another guideline is that the less dynamic the structural response the fewer sensors will be need to estimate the strain response.

The above discussion of Case 4 and Case 5 highlight the challenges of working with the AKF and this naturally leads to the key question of finding the optimal sensor placement given that the performance of the filter can depend heavily on the sensor placement. In the next section, the challenge of finding the optimal sensor placement is addressed.

4 Optimal sensor placement for model-based structural monitoring

The need for an optimal sensor placement arises naturally from the AKF formulation as only a limited number of selected measurements are used as the input for the filter. For the AKF to estimate statistically optimal states from a limited number of input measurements, it is essential that the measurements are able to provide good information about the system. The adage "garbage in, garbage out" is fitting for this problem since the better the sensor placement the better the resulting AKF estimation of the states. There are three main factors that need to be balanced for the sensor placement to be optimized. These factors are the number, type, location of the sensors. There are many secondary issues that also need to be addressed if a sensor network is to be deployed, a few of these secondary issues include how much redundancy should be added and the method for collecting the sensor data. A general overview of current sensor placement method and basic issues is written by Yi and Li. (Yi and Li, 2012)

The work presented here focuses on the optimization of the sensor location and number. To begin, it is necessary to consider the search space. Optimization of the sensor placement can be seen as a combinatorial optimization problem where for a given number of candidate locations, n, there is a number of, r, locations that can have sensors placed at them. Then the optimization of this problem with x number of combination can give the best results, i.e. optimized solution. The number of combinations can be calculated based on the Eqn. 30.

$$\#\ of\ combinations = \frac{n!}{(n-r)!\,(r)!} \tag{30}$$

In Eqn. 30, n is the number to be chosen from, it is based on the total number of possible locations and orientations of the sensors. For example, a strain sensor can be placed at any one location, i.e.

node, but it can also be placed at a specific orientation which gives certain strain component. Therefore, depending on the type of sensor the value of n can be different for the same structure. r is the number to be chosen, i.e. the number of sensors to be placed, and this value increases as more sensors are added.

For a simple example using the cantilever plate, the number of combinations can be calculated for two sensors using a 10×10 mesh this will give n as 121, i.e. total number of nodes, and r as 2, i.e. number of sensors to be placed; therefore, the number of combinations is found to 7,260. Adding 2 more sensors to the problem for a total of 4 sensors, so r equals 4, then the number of combinations increases to 8,495,410. These examples do not consider sensor orientation which will give a more rapid increase in the number of combinations, it is obvious that as the problem becomes more complicated making the use of an exhaustive search approach unfeasible. The computational time for the exhaustive search approach would be quite large so the best approach is to implement a search algorithm.

4.1 Genetic algorithm

A popular search algorithm that has been used for the optimization of sensor placement is the Genetic algorithm (GA). This algorithm was used successfully in the fields of mechanical and civil engineering. In the mechanical engineering field, GAs were used to find optimal locations for piezoelectric sensors and actuators for a composite plate (Kumar and Narayanan, 2007, Han and Lee, 1999) and the civil engineering field has seen GAs used to solve for the placement of tuned mass dampers in high rise buildings. (Abdullah et al., 2001) GAs are a type of all-purpose

population based stochastic search technique that applies the principles of natural selection and genetics. The main benefit of a GA is that it can efficiently find an optimal solution from complex and possibly discontinuous search space without requiring reformulation of the problem when evaluating possible solutions. (Mitchell, 1996)

To begin it is beneficial to introduce the basic terminology of a GA. Potential solutions are called individuals and are made up of chromosomes that contain the information specific to that individual. The groups of individuals are termed populations or generations. With a large population size, the genetic algorithm searches the solution space more thoroughly, thereby reducing the chance that the algorithm returns a local minimum that is not a global minimum. However, a large population size also causes the algorithm to run more slowly. After an initial generation is created then it is evolved over following generations using genetic operators called selection, elitism, crossover and mutation operators. The convergence of the population as each generation is ran leads to the optimal solution or individual. The evolution of the generations and the final result is called a run. Since the GA is stochastic search technique each run often produces a different result but careful tuning of the operators' parameters should reduce the difference between runs.

The most important component of the GA is the objective function, every individual is evaluated based on this function then assigned a fitness value. There are a variety of proposed objective functions for civil applications, i.e. Modal Assurance Criterion or Fisher Information Matrix which use modal shapes. (Yi and Li, 2012) These type of objective functions look at the modal shapes of

the structures and suffer from insensitivities to small differences. Since the goal of the research is looking at strain estimation which on the micro level these functions are unfeasible.

Therefore, the proposed objective function is unique to the optimization of strain estimation. This objective function evaluated each individual, i.e. proposed sensor placement, by using them as the input to the AKF to get the estimated response for a shortened time, 1/10 of a second was used to reduce the GA run time, after this the average strain error was calculated from Eqn 29 which is shown again here.

$$Error = \frac{\sqrt{\Sigma\left(\boldsymbol{\varepsilon}_{est} - \boldsymbol{\varepsilon}_{ref}\right)^2}}{Signal\ length} \tag{31}$$

If the individual is not a feasible, i.e. the response cannot be estimated for that sensor placement, then the fitness value was set to 100 so the individual would not be selected for reproduction. When the individual was feasible the average strain error of Eqn. 31 was set as the fitness value for that individual. The purpose of the GA is to minimize the fitness value and thereby minimize the average strain error.

The following discusses the details of the other genetic operators that were used. First is the selection operation, which specifies how the genetic algorithm chooses parents for the next generation. The purpose of the selection operator is to choose relatively 'fit' individuals to be part of the reproduction process. The chosen operator is the binary tournament selection. (Goldberg and Deb, 1991) Tournament selection selects parents by choosing *x* number of individuals at random, *x* is specified by the Tournament size, and then choosing the best individual out of that

set to be a parent. A tournament size of four is used for the GA used in this research. For more detail on the selection operator see Deb. (Deb, 2000)

Next is elitism where the individuals with the best fitness values in the current generation are guaranteed to survive to the next generation. These individuals are called elite children or elite count. At the end of run these top performing individuals will be considered the optimal solutions.

The next operator is the crossover operator, it combines two parents to form children for the next generation to explore the search space. The crossover function used is the intermediate function which can be described as a random weighted average of the parents. The child's chromosomes are enforced to be integers as part of the operator. A detailed description of the crossover function can be found from Deep et al. (Deep et al., 2009)

The mutation operator applies random changes to parents to form children. The mutation operator has an important role in maintaining adequate diversity in the population to avoid premature convergence. Adaptive feasibility function is used for mutation. The function randomly generates directions that are adaptive with respect to the last successful or unsuccessful generation. A step length is chosen along each direction so that linear constraints and bounds are satisfied. Mutation functions enforce variables to be integers. For details, see Deep et al. (Deep et al., 2009)

The following flowchart shows the process of the GA and where each of the operators would be used.

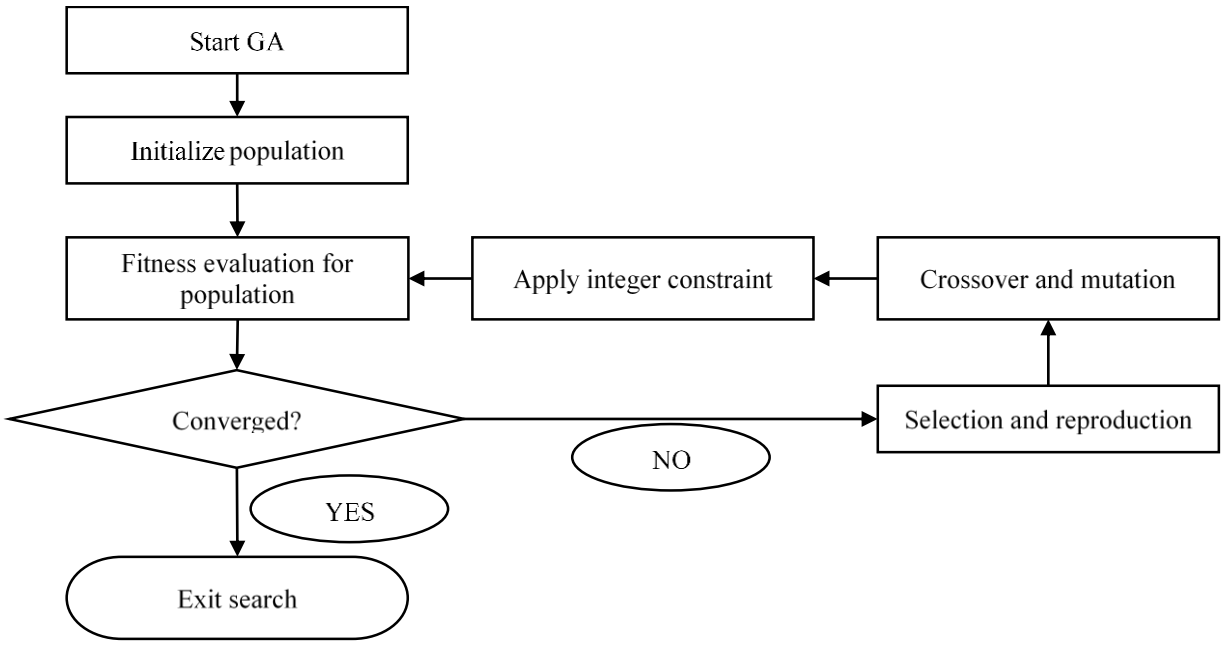

Figure 30: Flowchart of genetic algorithm

4.2 Genetic algorithm coding

The GA was implemented using the built-in Matlab Optimization Toolbox®. (Coleman and Zhang, 2015) The toolbox has several methods to search for global maximums or minimums. The GA provides several helpful properties making it an ideal choice for the problem to be solved here. The GA allows for easy customization including mixed-integer optimization. The problem to be solved falls into the mixed integer optimization category.

Mixed integer optimization is chosen because it is able to place the sensors at the node locations. Individuals were coded using three chromosomes. The first chromosome set the location on the x-axis and varied from 1 to 11, the second chromosome set the location on the y-axis and similarly varied from 1 to 11, and the third chromosome was used to set the orientation of the strain sensor

and varied from 0 to 2. To ensure the chromosomes were properly coded two different constraints were used. The first was an integer constraint which was applied using the mixed-integer optimization. The second constraint was to set lower and upper bounds on the chromosomes so values from 1 to 11 and 0 to 2 were selected. An example of how individuals were coded is shown; if a strain sensor is to be placed at node 1 to measure the ε_x then the individual would have the three chromosomes coded as: | 1 | 1 | 0 | and correspondingly a strain sensor placed at node 111 to measure ε_y is coded as: | 1 | 11 | 1 |.

The placement of multiple sensors on a structure can be done by using one of the following two approaches. The first approach is to consecutively place sensors, i.e. to place one sensor at a time and find the optimized location of the additional sensor to be placed. During this approach the previously placed sensors are considered fixed. This consecutive sensor placement has the disadvantage that the sensors placed first will affect the placement of future sensors. The effect this weighting has on sensor is not well studied for civil applications.

The second approach to place sensors, it to place them all at once. Then based on the results replace all the sensors again in an updated layout. This all-at-once approach is the method used in the developed GA. The advantage of this approach is that the placement will not be biased but the disadvantage is the increased search space. The large search space means that the run time of the search algorithm is also increased.

To exit the search, i.e. determine if convergence was met, two stopping criteria where used. The first criteria was to stop the search after the maximum number of generations was ran. This criteria

stops the search from running for an unlimited time and it necessary for problems was the search space is exceedingly large. The second criteria is the stall test where the search is stopped if the average fitness value change over a number of generations, 50 generations is this case, does not change more than a set tolerance level. That tolerance level is set to 1×10^{-6}. The tolerance value was set to be quite stringent so than exiting of the search is likely to be caused when the maximum number of generations is reached. This helps to ensure that the global minimum is found and the search will not be stopped early by a local minimum.

4.3 Numerical validation

The simulations were performed to test the performance of the GA and the same cantilever plate used for Case 1-4 was used. All properties, i.e. dimensions, Young's modulus, density, Poisson's ratio, and modal damping, remain the same as in these cases. 5% modeling error and 2% measurement noise is also included. As a reminder this plate structure is the smaller and stiffer of the previous two.

The cantilever plate was tested using the same input excitations and locations as Case 1-4. The purpose of keeping the similarities is to allow for the results found in this section to be compared to the previous cases.

Case 5: Near-optimal placement of 3 strain sensors

This case demonstrates the developed GA to find the near-optimal placement of 3 strain sensors on the cantilever plate. For the optimization problem with 3 strain sensor, the total possible number of combination is 7,906,261. This is calculated using r as 4 and n equal to 363 when strain orientation is accounted for, i.e. we can measure 1 of 3 different strain components for any one location. Given the large number of combinations this problem is best solved using the GA.

Several of the important parameters used in GAs are taken as follows:

Population size: 50

Length of chromosome: 9

Maximum number of generations: 100

Elite count: 2

Crossover probability: 0.8

Mutation probability: 0.16

(32)

For the optimization problem examined here there are three metrics considered to inform whether the GA is performing efficiently and a near global solution is found. The first metric is simply the convergence of the population which shows a minimum has been found. The second metric is the diversity of the population. A good amount of diversity in the population means that the search space is being thoroughly explored and the GA is not only examining one area of the search space. The third metric is the use of multiple runs. This is needed since the GA is a stochastic search technique and does not produce the same result every time. Therefore, it is advisable to do multiple runs for the same problem. The general convergence of the different runs helps to determine if the global minimum has been found and avoids local minimums. Four different runs are used in the 3 strain sensor problem.

The figure below shows the average fitness value of the population against the generation number for Run #2 from the GA.

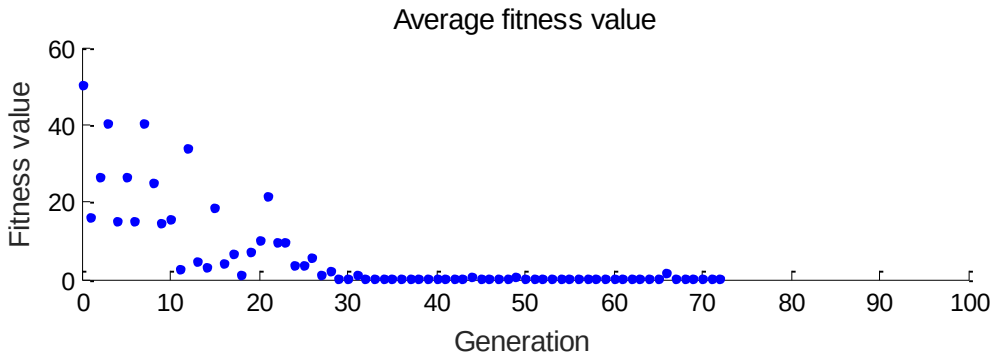

Figure 31: Average fitness value for Run # 2

The results shown in the figure above are representative of the other 3 runs. It is possible to see that the GA converges to the fittest solution during the run and that the search is ended because the stall test is met after 72 generations. It is also that noted that all of the runs were stopped by the stall test after running for 60 to 90 generations. Exiting from the stall test is preferred because then the search will not be exited prematurely and convergence can be assured. The figure below shows the best fitness value, i.e. lowest strain estimation error, found for the population at each generation for Run #2.

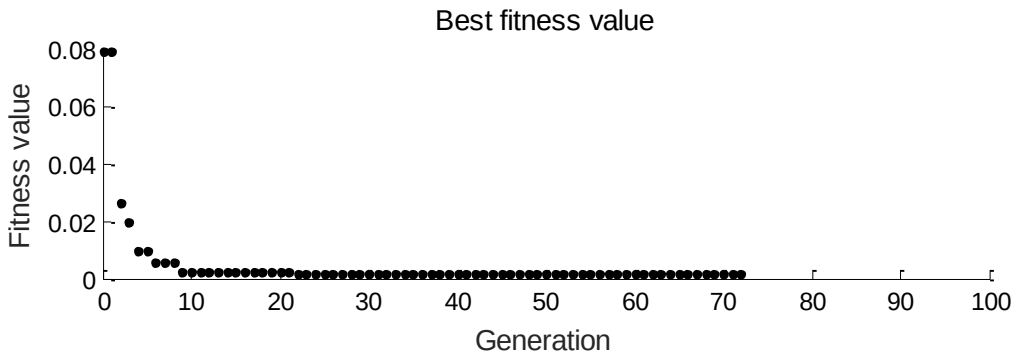

Figure 32: Best fitness value for Run # 2

Each drop in the figure means that a new sensor placement was found that had a lower strain estimation error. It is seen that after 22 generations the best fitness value remains constant, again representing the convergence of the search, until the search is ended by the stall test after 72 generations. Again, a similar results for the best fitness value was found for the other three runs.

The second metric that can be used to judge the performance of the genetic algorithm is the diversity of the population. The population's diversity can be represented using the average distance between individuals. If the average distance between individuals is large, then diversity is high; if the average distance is small, then diversity is low. Average distance is calculated as the average of a vector of distances of each individual in the generation to the nearest neighboring individual. The figure below shows a plot of the average distance for each generation versus the generation number for Run #2.

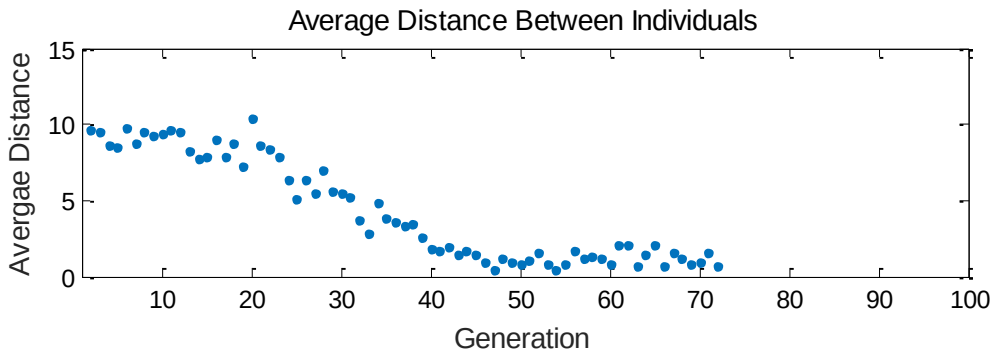

Figure 33: Average distance between individuals for Run # 2

In the figure above it is seen that the average distance between individuals starts around 10 and this is a good result because the maximum possible distance is 11. It is seen that a high average distance is maintained for approximately 20 generations and then the distance decreases. This is result is expected since the global minimum was found at 22 generations and once it is found the GA's diversity becomes lower as individuals converge. It is noted that the other three runs had similar trends for the average distance between individuals.

The third metric to show the efficiency of the GA is multiple runs. The results of the GA is best understood by visually seeing the relative locations where the GA placed the sensor. The figures below shown a summary of the 4 different runs which includes the average strain estimation error that the different sensor placements gave when ran for the full 6 second simulation time. Only three figures are shown because two of the runs produced the same sensor placements.

a.

Average μ-strain error = 0.0047

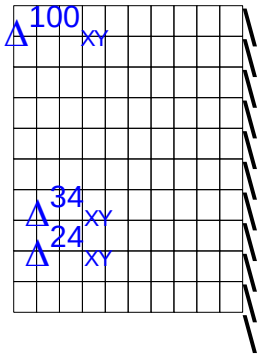

Strain measurement placement for Run # 1 and 3

b.

Average μ-strain error = 0.0039

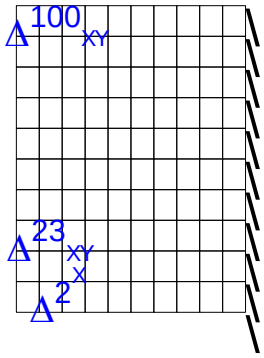

Strain measurement placement for Run # 2

c.

Average μ-strain error = 0.0036

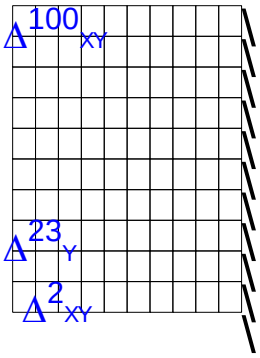

Strain measurement placement for Run # 4

Figure 34: Results for placement of three strain sensors

The results above show that a four runs gave a lower average strain estimation error then the previous strain measurement only simulations, i.e. Case 2. From the figure it is possible to see that the four runs gave similar locations for the sensor placement. To get better results, it is possible to the above results as the initial population and rerun the GA. Unfortunately, this method has not been explored here but the idea is that the search space has been reduced so rerunning the GA for a limited area can fine tune the sensor placement. For this work the results given by the four runs are satisfactory and a detailed investigation of the near-optimal placement found by the GA can be carried out.

First, the strain errors for all strain components and the average strain error for Run # 4 is shown in the figure below.

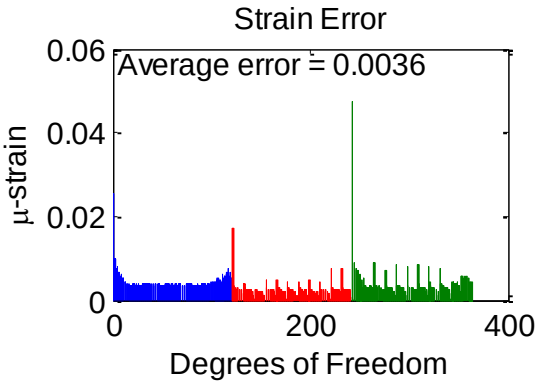

Figure 35: Error shown at all strain components for the near-optimal sensor placement

It can be seen from the above figure that the strain error values are small but there are a few trouble areas where the strain error is high compared to the other error values. This is one disadvantage of the objective function implemented here since the average strain error is minimized then it is possible that the error at a specific node may not be reduced. Further investigation into the trouble areas can be done using the strain history.

The figures below show the strain history and error values for the strain component, ε_x, at node 70 and for the shear strain component, γ_{xy}, at node 1, this is the area that gives the highest strain error, along with corresponding detailed views.

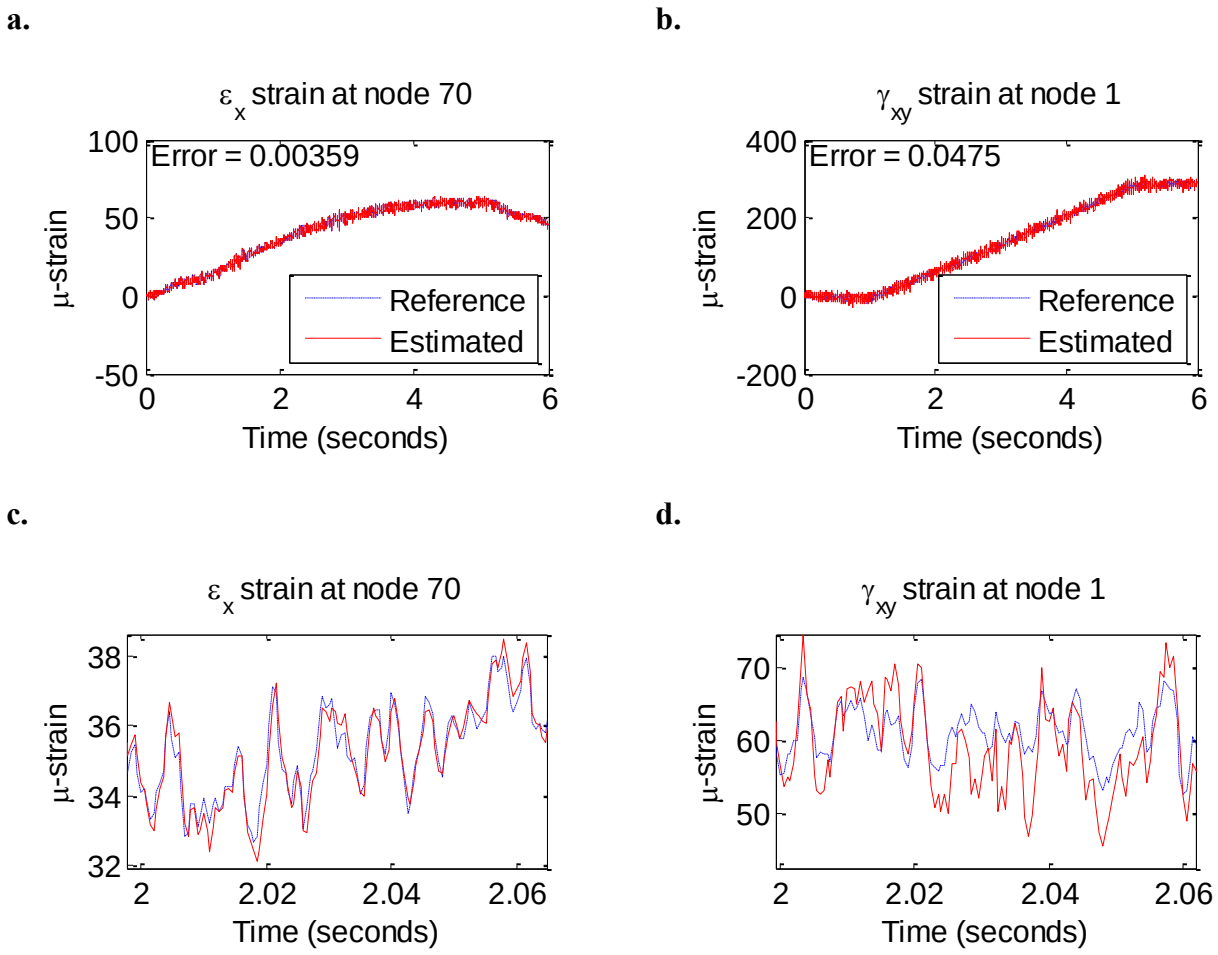

Figure 36: Complete, (a) (b), and detail, (c) (d), of the strain history for the near-optimal sensor placement

The figures above show drastically improved results if compared to Case 2, where strain measurements only were used as input to the AKF. This near-optimal case has an average strain error of 0.0036 micro-strain compared to 0.0066 micro-strain without optimization. Also from Figure 36.d it is seen that the near-optimized placement performs better at capturing the high frequency. This result is in contrast to the estimated strain at the same location in Case 2, Figure 13.d where the high frequency was not captured.

Comparing the near-optimal case to the multi-metric case, Case 3, it is see that the near-optimal case outperforms the multi-metric case considering the average strain error with 0.0036 micro-

strain to 0.00459 micro-strain, respectively. However, it is important to note that the multi-metric case can capture the high frequency so the trouble strain components with the large error values shown in Figure 35 are reduced, e.g. the γ_{xy} component at node 1 is 0.0475 micro-strain in the near-optimized case while only 0.0224 micro-strain in the multi-metric case.

If the result is looked at in the frequency domain as shown by the figure below, the increase in accuracy for the near-optimized case can be clearly seen as compared to the previous strain measurement only case.

a. **b.**

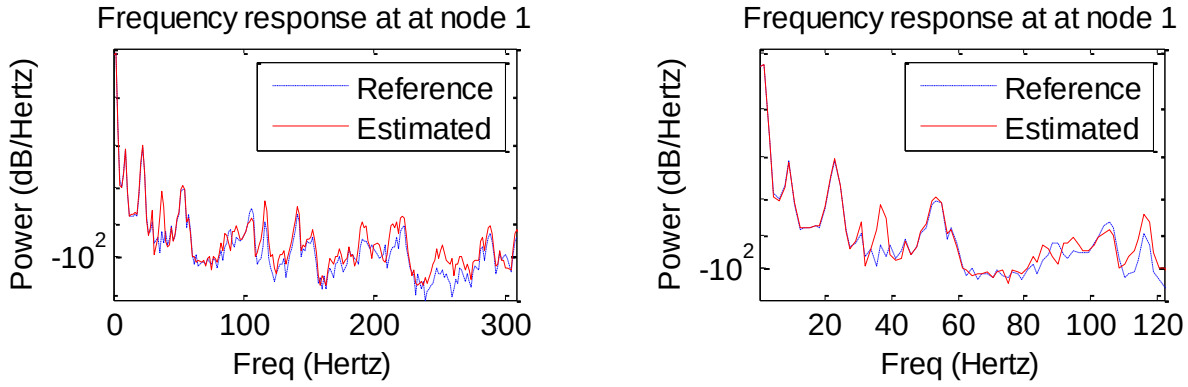

Figure 37: Complete (a) and detail (b) of the frequency response shown for the near-optimal sensor placement

However, the result is not perfect and it can be seen from the detailed view that one peak is falsely estimated at approximately 38 Hz. If compared to the multi-metric case, this false estimation does not occur.

Case 6: Limited return for increasing strain measurements

Case 6 uses the GA to investigate the effect of increasing the number of strain measurements. Based on experience it is suspected that there would be; a.) A minimum number of strain measurements needed for the AKF to work and b.) A decaying return, i.e. a smaller reduction in the average strain error, as the number of strain measurements are increased. The number of measurements is obviously going to be reliant on the structure, input excitation, and type of measurement. For the simulations here, the stiff cantilever plate from Cases 1-4 is used but hopefully the work here will be able to make some conclusions and provide a framework that can be applied generally.

For the plate considered, it is found that a minimum of three strain measurements were required to be used as input to the AKF. When two or fewer strain measurement were used for the input, the performance of the filter was very poor or the AKF couldn't solve the inverse problem. In the instance of poor performance, the filter did not have enough information to find the unique solution. This is one of the limitation of the AKF, where the filter will provide a false result if there is not enough information to find the unique solution. Information about solving the inverse problem can be found in the following references; (Welch and Bishop, 2006)

This means there is a lower bound on the number of sensors that are required for the AKF to be able to accurately predict the system states. This preliminary conclusion partly resolves the first factor of the optimization problem, number of sensors. It is clear that the lower bound on the number of sensors should be able to produce results with the resolution that is desired.

The table below show the average strain error as the number of strain measurements was increased from 3 to 8.

Table 2: Average strain error for different number of strain measurements

Number of strain measurements	Average strain error (μ-strain)
3	0.00360
4	0.00286
5	0.00241
8	0.00183

The table shows that the average strain error continues to decrease as the number of measurement used for the AKF input increases but the reduction in the error is not the same for each added measurement. The figure below displays the information from the table.

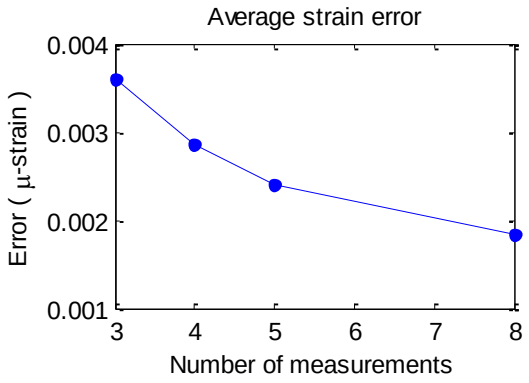

Figure 38: Average strain error for an increasing number of strain measurements

From the figure it is easy to see that the relationship between the average strain error value and the number of measurements is not linear. The relationship is a decaying function as more measurements are added. This shows that there is an upper bound on the number of sensors for which the benefit for each additional sensor begins to decreases. Eventually, the benefit per sensor may reach a limit where the cost of the sensor is larger than the benefit. The definition of upper

limit is ultimately at the discretion of the user and can be based on a cost-benefit analysis; however, this is not the research interest here.

4.4 Summary

The results show that when the GA is implemented to solve an integer constrained optimization problem with a very large number of possible combinations it is able to find near-optimized locations for the sensors. Since the GA is a stochastic search algorithm the term near-optimized is used to describe the sensor placements that were found since the verification/finding the true optimal sensor placement would require an exhaustive search which is improbable given the computational time.

However, the good performance of the GA is seen by using a couple of metrics to evaluate the performance. First, the use of multiple runs shows that proper tuning of the GA parameters leads to the convergence of the results, i.e. multiple runs end in sensors being placed at the same or adjacent locations. If necessary and as a part of future work, the results could be refined by setting some of the initial population of a run to these near-optimal locations and then running the search algorithm or alternatively, a user could use a simple trial and error process to refine sensor placement. Secondly, the performance of the GA can be evaluated by using the average distance between generations. When a high average distance between individuals is calculated for each generation of a run then this indicates that the population is diverse. The effect of a diverse population means the search space is being explored thoroughly, increasing the probability of finding the optimal solution.

The simulations in Case 5 show that sensor placements found have drastically reduced strain error values. The average strain error of the near-optimized case is approximately half of the trial and error optimized case, i.e. Case 2, where the values are 0.0036 and 0.006 respectively.

However, even with the improved results it is noted that the new sensor placement does not perform well at a few locations. In these locations, strain estimation of the high frequency component proves difficult when using strain measurements only as the input to the AKF. This is difficult can been seen in the frequency domain where estimated response has a false peak. To overcome this use of multi-metric input into the AKF works well at reducing error at these locations as shown in Case 3. Though optimization of the multi-metric case is not investigated as part of this research it would be of interest in the future and can be done without major modification, this being one benefit of the current GA.

This benefit of the GA, also allowed for the easy investigation into the effect that changing the number of strain measurements would have. In Case 6, the number of strain measurements used is increased from 3 to 8 to study the effect this would have of the strain estimation results. Some key conclusions are made, first is that a minimum of three strain sensors in needed for the AKF to be able to accurately estimate the strain response. Secondly, it is seen that as the number of strain measurements to be used as input to the AKF are increased that the decrease in the average strain error is not linear. This means that there is a limited return in accuracy for each additional sensor that is placed. Based on these conclusions, it can be stated that there is a minimum number of

measurements required to achieve accurate results from the AKF and there is a decaying return as more measurements are used as input.

5 Conclusions

A key goal of the research was to overcome the challenges of traditional SHM by using an alternative method to estimate the structural response at all locations by making use of a few measurements taken from the structure. This approach is advantageous since it is addresses the main difficulty of SHM for civil application which is the scale of the structures. The proposed approach is able to overcome the scale challenge by only needing a limited number of measurements and ideally theses measurement could be taken using reference-free sensors, i.e. strain and acceleration, thereby addressing the issue of costly installation and maintenance that often comes with instrumentation. This research identified plate structures as a structural element of significant importance but where there is no developed SHM method and where a lack of understanding has directly led to several structural failures. Furthermore, discussion of a SHM method for plate structures in the civil field is absent in the literature.

It is proposed that a hybrid approach can be used that combines a model, i.e. finite element model, of the structure along with the augmented Kalman filter, a linear recursive state estimator, which provides statistically optimized state estimates for all locations including unmeasured locations based on a limited number of sensor measurements. This hybrid approach uses a combination of the model and measurements to estimate the strain response in the presence of measurement noise and model error for the plate while using a minimal number of sensors and for multiple non zero mean excitations.

The simulation studies done as part of the research show that while both the measurement noise and model error effect the accuracy of the strain estimation, it is seen that model error has a greater effect. The effect of using different types of sensors is then investigated, the use of acceleration measurements only as input to the AKF provides unstable results when applying non-zero mean excitations along with measurement noise and model error. However, the use of acceleration measurements can provide good information about the response of the structure on a global level and for the high frequency response which makes it a valuable measurement if it can be stabilized. This result is similar to other previous work that investigated different structural elements, i.e. trusses and beams. Next, if strain measurements only are used as input, it provides good stable information and is able to directly give information about the strain locally. It can capture the low frequency of the excitation accurately. However, this case has trouble estimating the high frequency component.

The previous results show the weakness of relying on only one type of measurement and make the use of multi-metric data as an input to the AKF appealing since the strengths of different sensors can be combined. The first advantage of multi-metric data is that the acceleration measurements become stable. Then the information provided by the acceleration measurement improves the results in the high frequencies and gives information about the system on global level. The multi-metric data also takes advantage of the strain measurements to capture low frequency changes allowing the AKF to work for non-zero mean excitations. However, when using multi-metric data it is important to understand the effect of placement, number, and type of sensors. An example of the importance of sensor placement is given by Case 4 where an arbitrary sensor placement gives

bad strain estimations. Also for sensor placement a good understanding of the structural characteristics will help with finding the optimal sensor layout.

The simulation from the flexible plate, i.e. Case 5, demonstrate the importance of structural characteristics and revel that multi-metric input is not always the best. The structural characteristics are important in determining the required number and type of measurements needed for the AKF. Lower frequency structures will need a fewer number of sensors and since they lack a high frequency response acceleration measurements are not as informative. The simulated plate was able to provide accurate strain estimation with only 2 strain measurement as input but bad estimation occurred when 1 strain and 1 acceleration where used as input.

The research into the AKF showed the need for sensor placement optimization if the best results are to be achieved. The key challenge to sensor optimization is the large search space and being able to find the potential solutions while reducing the required computational time. To accomplish this a framework was established using a search algorithm, i.e. genetic algorithm (GA), for optimizing sensor placement. The use of a GA has several advantages when compared to other search algorithms. A key advantage is that the problem does not have to be reformulated for each search. This allows for the same GA to be used for optimization of problems with different numbers or types of sensors.

The GA that was implemented was used to investigate the placement of strain sensors for plate structures. The objective of the GA was to minimize the average strain error value as calculated using Eqn. 31. The GA was able to find a near-optimized sensor placement for 3 strain sensors.

This new layout provides results that are drastically improved from the previous case of strain measurement only, i.e. Case 2, where placement was done using experience and a trial and error process. The average strain error was reduced from 0.0066 micro-strain to 0.0036 micro-strain between the two cases. However, the near-optimized strain sensor placement had problems capturing the high frequency component of the response at a few locations. This difficulty is a general weakness of the strain measurement only case and in this regard the multi-metric case was able to reduce the error at the locations where the strain measurement only case had trouble.

The GA was also used to investigate the effect of changing the number of strain sensors. The number of strain measurement used for the AKF was increased from 3 to 8. It was found that a minimum number of measurements was required for the filter to give accurate results and for the simulated stiff plate structure 3 strain measurement were required. In contrast, the flexible plate used in Case 5 only required 2 strain measurements to be as input to the AKF to obtain accurate results. This is due to the structural characteristics as previously explained. When the number of strain measurements was increased it was observed that the return, i.e. decrease in average strain error, was not linearly related to the number of measurements. The impact of this is that there is a finite number of strain measurement that can be used before there will be no noticeable increase in the accuracy of strain. Based on this it is likely that a cost-benefit analysis will control the number of sensors to be placed as the cost of placing another sensor will not offset the increase in accuracy.

The overall conclusion of the simulations show that it is possible to use the AKF to accurately estimate the strain values for the entire plate structure using a limited number of sensors. The AKF

approach is robust and works for non-zero mean excitations with measurement noise and model error in the system. It is found that measurement input to the AKF is dependent on structural characteristics. The number, type and locations of these measurements is variable but the use of a sensor optimization scheme can be used to place the sensors. It is proposed that a GA would be the best approach because many different optimizations can be done with minimal changes to the algorithm between runs.

Basically, this research into plate structures using the AKF is able to improve an area that has not been developed in the literature. It also provides a good framework for the expansion of the AKF method to other structural elements and to fieldwork. For example, the work done here provides an approach that can be used in the field to determining the placement of the sensors when using the AKF. In the overall scheme, being able to accurately estimate strain using the AKF approach has the potential to be used in structural health monitoring method.

5.1 Area of future work

There are several areas of future work that can be done to expand the body of work done here. The first area that needs to be carried out is laboratory scale experimentation to demonstrate that the results of the simulations can recreated using a real system. The cantilever plate test setup can be used for the laboratory scale experiment which is an additional reason why this setup was chosen. The experiment would be done using a shaker table to apply exact, and known excitations, then sensors attached to the plate would feed information to a data acquisition system. The different scenarios could be carried out with selected measurements used as the input for the AKF and the

estimated strain values then compared to additional measurements taken on the structure. These additional measurements would be used as the reference and not be provide in the input into the AKF.

Another key area of future work, is the extension of this AKF approach to the complicated shell element. This would allow the incorporation of in-plane behavior in the finite element model but increases the total degrees of freedom to 6. The use of this type of element would require an in-depth review of available literature and careful selection of a finite element theory to construct the element. This care is needed since there is overall consensus on an acceptable general finite element formulation for shell elements. A summary of the challenges that researchers are facing on this topic can be found in the Chapelle and Bathe, 1998. (Chapelle and Bathe, 1998)

Additionally, the area of optimal sensor placement could be further explored using GA framework established here. The further work would look into the performance of a variety of different sensor layouts, i.e. optimized multi-metric placement. It would also be of interest to apply the GA optimization approach to the other structures to see its performance, e.g. optimizing sensor placement for trusses or beams that are used in the AKF approach.

References

Abdullah, M. M., Richardson, A., and Hanif, J. (2001). "Placement of sensors/actuators on civil structures using genetic algorithms," Earthquake Engineering & Structural Dynamics, 30(8), 1167-1184.

Ayzazyan, H., Stahmer, J., Vellozzi, J. (1989). “National Radio Astronomy Observatory 300 Foot Telescope,” Ammann & Whitney Consulting Engineers, New York, New York, Tech. Rep.

Bathe, K.J. (1982). [Finite element procedures in engineering analysis]. Englewood Cliffs, NJ. Prentice-Hall.

Brownjohn, J. M. W. (2007), “Structural health monitoring of civil infrastructure. Philosophical Transactions of the Royal Society A," Mathematical, Physical and Engineering Sciences, 365, 589-622.

Chapelle†, D., & Bathe, K. J. (1998). “Fundamental considerations for the finite element analysis of shell structures,” Computers and Structures, 66(1), 19-36.

Coleman, T., and Zhang, Y. (2015). "Optimization toolbox for use with matlab," Natick, MA. The MathWorks, Inc.

Deb, K. (2000). "An efficient constraint handling method for genetic algorithms," Computer Methods in Applied Mechanics and Engineering, 186(2–4), pp. 311–338.

Deep, K., Singh, K.P., Kansal, M.L., and Mohan, C. (2009). "A real coded genetic algorithm for solving integer and mixed integer optimization problems," Applied Mathematics and Computation, 212(2), pp. 505–518.

Doebling SW, Farrar CR, Prime MB, Shevitz DW. (1996). "Damage identification and health monitoring of structural and mechanical systems from changes in their vibration characteristics: A literature review," Los Alamos National Lab., NM (United States).

Farrar, C. R. (2001), "Historical overview of structural health monitoring," Lecture Notes on Structural Health Monitoring using Statistical Pattern Recognition.

Fatemi, A. and Yang, L. (1998). "Cumulative fatigue damage and life prediction theories: a survey of the state of the art for homogeneous materials," Int J Fatigue 20(1), 9–34.

Ferreira, A. J. M. (António J. M.). (2008). [MATLAB codes for finite element analysis: Solids and structures], Dordrecht; London, Springer.

FHWA. (2012) "New ways to predict bridge performance," Exploratory Advanced Research Program. Federal Highway Administration. U.S. Department of Transportation. Publication No. FHWA-HRT-10-062 HRTM-04/07-10(1M)E

Ghajari, M., Z. Sharif-Khodaei, M. H. Aliabadi, and A. Apicella. (2013). "Identification of impact force for smart composite stiffened panels." Smart Materials and Structures 22(8), 085014.

Goldberg, D.E., Deb, K. (1991). "A comparison of selection schemes used in genetic algorithms, in: Foundations of Genetic Algorithms," 1, FOGA-1, vol. 1, pp. 69–93.

Han, J., and Lee, I. (1999). "Optimal placement of piezoelectric sensors and actuators for vibration control of a composite plate using genetic algorithms," Smart Materials and Structures, 8, 257.

Hill, H.J., McGormley, J.C., Koob, M.J., Nugent, W.J. (2008). "I-35W Bridge over the Mississippi River: Collapse Investigation," Wiss, Janney, Elstner Associates, Inc., Northbrook, Illinois, Tech. Rep. 2007.3702.

Jang, S., Jo, H., Cho, S., Mechitov, K., Rice, J. A., Sim, S. H., ... & Agha, G. (2010). "Structural health monitoring of a cable-stayed bridge using smart sensor technology: deployment and evaluation," Smart Structures and Systems, 6(5-6), 439-459.

Jo, H., and Spencer Jr, B. F. (2014). "Multi-metric model-based structural health monitoring," Proc. SPIE 9061.

Kuhn, B., Lukic, M., Nussbaumer, A., Gunther, H.-P., Helmerich, R., Herion, S., Kolstein, M.H., Walbridge, S., Androic, B., Dijkstra, O., and Bucak, O. (2008). “Assessment of Existing Steel Structures: Recommendations for Estimation of Remaining Fatigue Life,” Joint Report Prepared under the JRC-ECCS cooperation agreement for the evolution of Eurocode.

Kumar, K.R., and Narayanan, S. (2007). "The optimal location of piezoelectric actuators and sensors for vibration control of plates," Smart Materials and Structures, 16(6), 2680-2691

Lourens, E., Reynders, E., De Roeck, G., Degrande, G. and Lombaert, G. (2012). “An augmented Kalman filter for force identification in structural dynamics,” Mechanical Systems and Signal Processing, 27(1), 446-460.

Lynch, J.P., & Loh, K.J. (2006), “A summary review of wireless sensors and sensor networks for structural health monitoring," The Shock and Vibration Digest, 38(2), 91-28.

Mitchell, M. (1996). [An Introduction to Genetic Algorithms]. Cambridge, MA. A Bradford Book.

Naets, Frank, Javier Cuadrado, and Wim Desmet. (2015). "Stable force identification in structural dynamics using Kalman filtering and dummy-measurements." Mechanical Systems and Signal Processing 50, 235-248.

Palanisamy, R., Cho, S., Kim, H., & Sim, S. (2015). “Experimental validation of Kalman filter-based strain estimation in structures subjected to non-zero mean input,” Smart Structures and Systems, 15(2), 489-503.

Papadimitriou, C., Fritzen, C., Kraemer, P., and Ntotsios, E. (2011). “Fatigue predictions in entire body of metallic structures from a limited number of vibration sensors using Kalman filtering,” Structural Control and Health Monitoring, 18(5), 554-573.

Sohn, H., Farrar, C. R., Hemez, F. M., Shunk, D. D., Stinemates, D. W. and Nadler B. R. (2003). “A review of structural health monitoring literature: 1996-2001," Los Alamos National Lab., NM (United States). Tech. Report, LA-13976-MS.

Spencer Jr., B.F., Jo, H., Mechitov, K.A., Li, J., Sim, S.H., Kim, R.E., Cho, S., Linderman, L.E., Moinzadeh, P., Giles, R.K., and Agha, G. (2015), "Recent Advances in Wiress Smart Sensors for Multi-scale Monitoring and Control of Civil Infrastructure," Journal of Civil Structural Health Monitoring, Published online ahead of print.

Spencer, B. F., Ruiz-Sandoval, M. E., and Kurata, N. (2004). "Smart sensing technology: Opportunities and challenges," Structural Control and Health Monitoring, 11(4), 349-368.

Welch, G. and Bishop, G. (2000). “An introduction to the Kalman filter,” Dept. Comput. Sci., Univ. North Carolina, Chapel Hill, Tech. Rep. TR95041.

Whitmore, R. E. (1952). “Experimental Investigation of Stresses in Gusset Plates,” Engineering Experiment Station, University of Tennessee, Knoxville, TN, Bulletin No. 16.

Wright, F.G., (2007). "Immediate inspection of deck truss bridges containing Fracture Critical Members (FCM)," Federal Highway Administration, U.S. Department of Transportation. Technical Advisory 5140.27.

Yi, T., & Li, H. (2012). “Methodology developments in sensor placement for health monitoring of civil infrastructures,” International Journal of Distributed Sensor Networks, 2012, 1-11.

Zhou, Y.E. (2008). “Assessment of bridge remaining fatigue life through field strain measurement,” Journal of Bridge Engineering-ASCE 11(6), 737-744.